ANTIOXIDANTS & REDOX SIGNALING
Volume 17, Number 8, 2012
© Mary Ann Liebert, Inc.
DOI: 10.1089/ars.2011.4288

ORIGINAL RESEARCH COMMUNICATION

Targeted Deletion of *Nrf2* Impairs Lung Development and Oxidant Injury in Neonatal Mice

Hye-Youn Cho,[1] Bennett van Houten,[2] Xuting Wang,[3] Laura Miller-DeGraff,[1] Jennifer Fostel,[1] Wesley Gladwell,[1] Ligon Perrow,[1] Vijayalakshmi Panduri,[3] Lester Kobzik,[4] Masayuki Yamamoto,[5] Douglas A. Bell,[3] and Steven R. Kleeberger[1]

Abstract

Aims: Nrf2 is an essential transcription factor for protection against oxidant disorders. However, its role in organ development and neonatal disease has received little attention. Therapeutically administered oxygen has been considered to contribute to bronchopulmonary dysplasia (BPD) in prematurity. The current study was performed to determine Nrf2-mediated molecular events during saccular-to-alveolar lung maturation, and the role of Nrf2 in the pathogenesis of hyperoxic lung injury using newborn *Nrf2*-deficient ($Nrf2^{-/-}$) and wild-type ($Nrf2^{+/+}$) mice. ***Results:*** Pulmonary basal expression of cell cycle, redox balance, and lipid/carbohydrate metabolism genes was lower while lymphocyte immunity genes were more highly expressed in $Nrf2^{-/-}$ neonates than in $Nrf2^{+/+}$ neonates. Hyperoxia-induced phenotypes, including mortality, arrest of saccular-to-alveolar transition, and lung edema, and inflammation accompanying DNA damage and tissue oxidation were significantly more severe in $Nrf2^{-/-}$ neonates than in $Nrf2^{+/+}$ neonates. During lung injury pathogenesis, Nrf2 orchestrated expression of lung genes involved in organ injury and morphology, cellular growth/proliferation, vasculature development, immune response, and cell–cell interaction. Bioinformatic identification of Nrf2 binding motifs and augmented hyperoxia-induced inflammation in genetically deficient neonates supported *Gpx2* and *Marco* as Nrf2 effectors. ***Innovation:*** This investigation used lung transcriptomics and gene targeted mice to identify novel molecular events during saccular-to-alveolar stage transition and to elucidate Nrf2 downstream mechanisms in protection from hyperoxia-induced injury in neonate mouse lungs. ***Conclusion:*** *Nrf2* deficiency augmented lung injury and arrest of alveolarization caused by hyperoxia during the newborn period. Results suggest a therapeutic potential of specific Nrf2 activators for oxidative stress-associated neonatal disorders including BPD. *Antioxid. Redox Signal*. 17, 1066–1082.

Introduction

Extensive lung development takes place in preterm infants born at 24–36 weeks of gestation with body weight <1000 g (47). Critical morphologic processes in this saccular phase include widening of distal airways to prepare subsequent formation of alveoli, differentiation of type 1 and 2 cells, and thinning of the air–blood barrier. Bronchopulmonary dysplasia (BPD) is a chronic lung disease and common outcome developing in about 20% of the very low birth weight premature infants born at the saccular phase of lung development each year in the United States (3).

The risk of BPD in these cohorts is inversely proportional to the gestational age at birth (25). Major pathologic features of BPD are failure in alveolarization leading to simplified air space and lowered alveolar density, inflammation, and respiratory distress. Lung injury in BPD is thought to result from early developmental arrest probably associated with prenatal exposure or genetic factors and interrupting alveolar growth as observed in extreme prematurity ("new" BPD), or from structural damage of relatively more developed saccular lungs characterized by surfactant deficiency ("old" BPD) that receive respiratory support with mechanical ventilation and prolonged oxygenation (3). BPD survivors often have

[1]Laboratory of Respiratory Biology, National Institute of Environmental Health Sciences, National Institutes of Health, Research Triangle Park, North Carolina.
[2]Department of Pharmacology and Chemical Biology, University of Pittsburgh School of Medicine and Hillman Cancer Center, Pittsburgh, Pennsylvania.
[3]Laboratory of Molecular Genetics, National Institute of Environmental Health Sciences, National Institutes of Health, Research Triangle Park, North Carolina.
[4]Department of Environmental Health, Harvard University School of Public Health, Boston, Massachusetts.
[5]Tohoku University Graduate School of Medicine, Sendai, Japan.

Innovation

The current study is the first to use lung transcriptomic and pathway analyses to understand the role of Nrf2 in the molecular events during saccular-to-alveolar stage transition. Transcriptome analysis of lungs from $Nrf2^{-/-}$ and $Nrf2^{+/+}$ mice also supported a functional role for Nrf2 and related downstream effector mechanisms (*e.g.*, *Gpx2* and *Marco*) in the pathogenesis of hyperoxia-induced lung injury in neonates. Results collectively provide insights into Nrf2-driven host defense mechanisms in developing lung, and suggest a therapeutic potential of specific Nrf2 activators in bronchopulmonary dysplasia and other neonatal diseases associated with oxidative stress (*e.g.*, respiratory syncytial virus disease).

clinically significant respiratory symptoms and functional abnormalities that persist into adolescence and early adulthood, indicating lifelong consequences of BPD (33).

Hyperoxia-induced injury in underdeveloped lungs of newborn rodents has been investigated as a model for BPD (49). Angiogenesis proteins including vascular endothelial growth factor (VEGF) (27, 43), keratinocyte growth factor (20), and matrix metalloproteases (MMPs) including MMP-9 (29), are essential in lung development to protect against BPD pathogenesis. In contrast, cathepsin S (23), transforming growth factor beta (TGF-β) (46), or cytokines such as interleukin 1β (7) contribute to lung injury in experimental BPD.

Therapeutically administered hyperoxia to premature infants has been considered to be one contributing cause of BPD, and reactive oxygen species (ROS) are implicated in its pathogenesis (6, 17). NF-E2 related factor 2 (Nfe2l2, Nrf2), a transcription factor for antioxidant response element (ARE)-mediated antioxidant and defense gene expression (24), is essential in tissue protection (26). Using adult mice genetically deficient in *Nrf2* ($Nrf2^{-/-}$), a protective role of Nrf2 and ARE-responsive effector genes has been shown in oxidant-mediated lung injury (9, 12, 13, 16, 36, 37, 44).

The current study was designed to identify Nrf2-mediated molecular events during the late-phase lung maturation, and determine the role of Nrf2 in the pathogenesis of hyperoxia-induced injury in neonatal mouse lungs. For this purpose, transcriptome analysis revealed lung gene expression profiles from saccular stage (postnatal days P1–P3) and more mature late saccular/early alveolar phase (P4) that differed between newborn $Nrf2^{+/+}$ and $Nrf2^{-/-}$ mice. We also exposed $Nrf2^{+/+}$ and $Nrf2^{-/-}$ mice to hyperoxia during early postnatal ages (P1–P4), and differential susceptibility to lung injury and abnormal alveolarization were found. Lung microarray gene profiling and computerized algorithmic screening for ARE characterized potential downstream mechanisms of Nrf2-mediated protection against development of hyperoxia-induced lung injury.

Results

Saccular lung maturation during P1–P4

Developmental lung gene expression profiles. Statistics-based analysis (Fig. 1A) and visual data mining (Fig. 1B) determined the greatest transcriptome differences between P1 and P4 during early postnatal period in $Nrf2^{+/+}$ neonates. Among significantly varied genes ($n = 1674$, $p < 0.01$) between saccular stage (*i.e.*, P1–P3) and late saccular/alveolar stage (*i.e.*, P4), 324 transcripts were lower (by $\geq 50\%$) at P1–P3 (mostly P1 and/or P2) than at P4. They encoded genes for multiple centromere proteins, kinesin family members, cyclins, and DNA polymerases associated with cell cycle (DNA replication, recombination, and repair), cellular assembly, and epigenetic pathways (Fig. 1A–C and Supplementary Table S1A; Supplementary Data are available online at www.liebertonline.com/ars). Consistent with message profiles, proliferating cell nuclear antigen (PCNA), a DNA replication and cell proliferation marker, was lower at P1 compared with other postnatal days (Fig. 1D). Postnatal age-dependent increase in PCNA was obvious in endothelial and epithelial cells (Fig. 1D). Conversely, expression of 198 transcripts was ≥ 2-fold higher at birth (192 genes higher only at P1, none at P3) compared with P4 (Fig. 1A–C and Supplementary Table S1B). These included genes encoding transmembrane and junction proteins and antioxidants associated with the network of connective tissue and skeletal/muscular system development and function.

Saccular-to-alveolar transition of postnatal lungs. Normal lung maturation in $Nrf2^{+/+}$ newborns (Table 1) was characterized by saccular-to-alveolar transition from simple, poorly septated saccules at P1 (stage 1) to simple septation of saccules at P3 (stage 2) and the appearance of branched septa and multilobular alveoli at P4 (stage 3). Branched septi/alveoli were evident at P4 in the majority of neonates (67%). Lung maturation in $Nrf2^{-/-}$ newborns was comparable to $Nrf2^{+/+}$ newborns with branched septi/multilobular alveoli present in 75% of mice by age P4 (Table 1).

Role of Nrf2 in developmental lung transcriptome. *Nrf2* deficiency significantly affected expression of 9737 transcripts during P1–P4; these transcripts have roles mainly in tissue and organ development, cancer, cell death, and infectious disease and mechanism (Fig. 2A). Transcripts constitutively lower ($\geq 50\%$) in $Nrf2^{-/-}$ than in $Nrf2^{+/+}$ neonates (Fig. 2B and Supplementary Table S2A) were networked in DNA replication, recombination, and repair; tissue development; lipid metabolism; and redox cycle and stress response pathways. In contrast, several genes associated with immunity, lymphatic system development, and cell–cell interaction networks were expressed higher in $Nrf2^{-/-}$ than in $Nrf2^{+/+}$ at P1–P4 (Fig. 2B and Supplementary Table S2B). Visual profile analysis also revealed distinct patterns of Nrf2-dependent transcript expression (Fig. 2C and Supplementary Table S3). Profile 1 included transcripts (*e.g.*, *Ifi44* and *Tcf7*) markedly upregulated at P2 in $Nrf2^{-/-}$ mice; profile 2 included transcripts (*e.g.*, *Myh* and *Tnn*) overexpressed at P2–P3 in both genotypes, but more highly in $Nrf2^{-/-}$ mice; and transcripts in profile 3 (*e.g.*, *Aox1*, *Clstn2*, and *Sbf2*) were totally attenuated in $Nrf2^{-/-}$ mice.

Role of Nrf2 in hyperoxia-induced lung injury phenotypes

Growth and mortality of neonates. Hyperoxia retarded growth as indicated by lower body weight than air exposure in both genotypes after 100% and 70% O_2 (Fig. 3A). However, suppression of weight gain was significantly greater in $Nrf2^{-/-}$ than in $Nrf2^{+/+}$ mice (Fig. 3A). Hyperoxia (100%) also

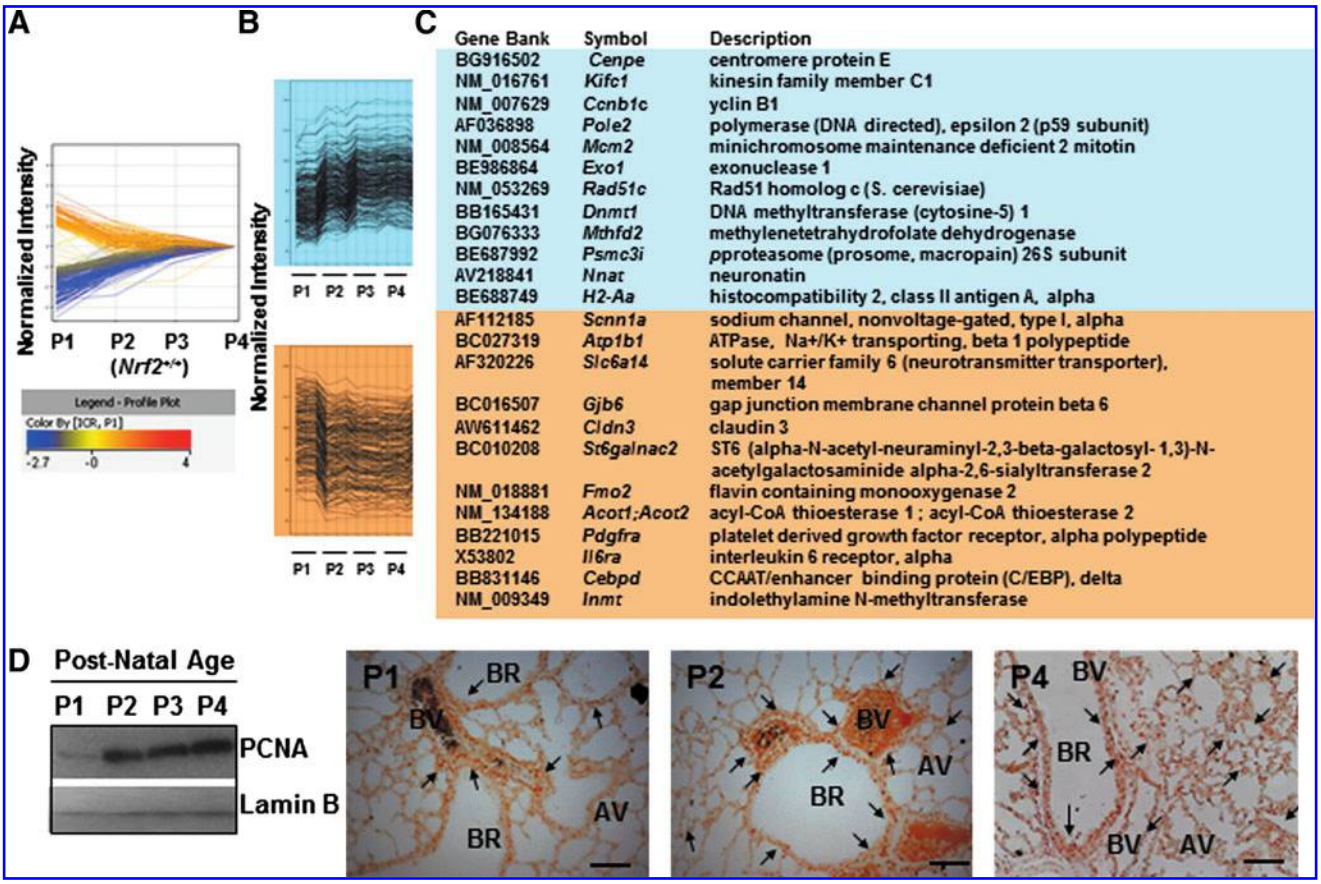

FIG. 1. Gene expression profiles during postnatal lung development. (A) Expression kinetics of ≥2-fold suppressed ($n=324$, *blue*) or upregulated ($n=198$, *orange-red*) genes at P1–P3 relative to age P4 in $Nrf2^{+/+}$ mice ($p<0.01$). Average transcript levels of individual genes at each time were normalized to those at P4. *Color bar* indicates average expression intensity. **(B)** Differential transcript expression patterns during P1–P4 in $Nrf2^{+/+}$ and $Nrf2^{-/-}$ mice were identified by visual data mining (Spotfire). Signal intensity of individual sample transcript (*each vertical line*) is indicated as log2-normalized value. **(C)** Selected differentially expressed genes (≥2-fold, from Supplementary Tables S1A, B) are presented. Genes in blue or in orange are ≥2-fold lower or higher, respectively, at least one time during P1–P3 than in P4. **(D)** Suppression of lung proliferating cell nuclear antigen (PCNA) at P1 relative to later postnatal times was confirmed by Western blotting and immunohistochemistry in $Nrf2^{+/+}$ mice. Nuclear lamin B level was determined as a loading control. PCNA-positive nuclei were histologically detected in pulmonary artery and main stem bronchi, and the populations were increased throughout the lungs by P4 (P3 tissues not shown). *Arrows*, PCNA-stained cells. AV, alveoli; BR, bronchiole; BV, blood vessel. Representative light photomicrographs are shown ($n=3$/group). Bars indicate 100 μm. (To see this illustration in color the reader is referred to the web version of this article at www.liebertonline.com/ars)

caused greater mortality in $Nrf2^{-/-}$ mice relative to $Nrf2^{+/+}$ mice (Fig. 3B). Seventy percent hyperoxia did not cause death of any neonatal mice.

Lung injury and inflammation. Minimal-to-mild inflammation was found in control mice of both genotypes exposed to room air (Table 1). Hyperoxia (100%, 3 days) caused significant pulmonary protein edema as assessed by increased protein concentration and cellular inflammation (neutrophils and monocytes) in bronchoalveolar lavage (BAL) fluids from $Nrf2^{+/+}$ and $Nrf2^{-/-}$ neonates (Fig. 3C). Compared with $Nrf2^{+/+}$mice, more necrotic (lysis) and apoptotic (nuclear fragmentation) cells were found in BAL returns from $Nrf2^{-/-}$ mice (Fig. 3D, E, no deoxynucleotidyl transferase-mediated dUTP nick-end labeling [TUNEL]-positive cells detected in air controls). Protein exudation in air spaces, alveolar inflammation and disruption, and perivascular-peribronchiolar edema were more severe and frequent in $Nrf2^{-/-}$ neonates relative to $Nrf2^{+/+}$ neonates after 3 days of 100% O_2. Hyperoxia caused exudative-phase diffuse alveolar damage in 50% of $Nrf2^{-/-}$ lungs examined, while no lungs from $Nrf2^{+/+}$ mice had this severe pathology (Fig. 3F and Table 1). Alveolar development in $Nrf2^{+/+}$ mice after 3 days of 100% O_2 was comparable to their air controls with branched septi and alveoli present in 67% of mice (stage 3, Table 1). However, relatively fewer $Nrf2^{-/-}$ neonates had developing multilobular alveoli and branched septi at 3 days after 100% O_2 (stage 3: 2/8; stage 2: 6/8), indicating a delay in alveolar maturation (Table 1). Consistent with the histopathologic findings, radial alveolar count (RAC) determined that hyperoxia exposure caused significant alveolar simplification in both genotypes of mice, but RAC was significantly lower in $Nrf2^{-/-}$ neonates relative to $Nrf2^{+/+}$ neonates after hyperoxia (Supplementary Fig. S1). Mild hyperplasic changes in airway epithelium of both strains and mild-to-moderate perivascular and peribronchiolar edema in $Nrf2^{-/-}$ neonates were found after 70% O_2, while BAL parameters were not significantly altered by 70% O_2 in either genotype (data not shown). Because 70% O_2

Table 1. Differential Alveolar Maturation Status and Hyperoxia-Induced Airway Lesions in *Nrf2*$^{+/+}$ and *Nrf2*$^{-/-}$ Neonates During Postnatal Days

Postnatal age (exposure day)	*Saccular-to-alveolar transition*[a]	*Air*		*100% O_2*	
		Nrf2$^{+/+}$	*Nrf2*$^{-/-}$	*Nrf2*$^{+/+}$	*Nrf2*$^{-/-}$
P1 (0 day)	Stage 1	2/2[b]	4/4	—	—
	Stage 2	0	0	—	—
	Stage 3	0	0	—	—
P2 (1 day)	Stage 1	1/3	0	0	1/3
	Stage 2	2/3	3/3	2/2	2/3
	Stage 3	0	0	0	0
P3 (2 days)	Stage 1	0	1/3	0	0
	Stage 2	3/3	1/3	2/2	4/4
	Stage 3	0	1/3	0	0
P4 (3 days)	Stage 1	0	0	0	0
	Stage 2	1/3	2/8	3/9	6/8
	Stage 3	2/3	6/8	6/9	2/8

		Air						*100% O_2*					
		Nrf2$^{+/+}$			*Nrf2*$^{-/-}$			*Nrf2*$^{+/+}$			*Nrf2*$^{-/-}$		
Postnatal age (exposure day)	*Injury score*[c]	II	AE	AI	II	AE	AI	II	AE	AI	II	AE	AI
P2 (1 d)	0	0	3/3	3/3	0	3/3	3/3	2/2	2/2	2/2	1/3	3/3	3/3
	1	3/3	0	0	2/3	0	0	0	0	0	1/3	0	0
	2	0	0	0	1/3	0	0	0	0	0	1/3	0	0
	3	0	0	0	0	0	0	0	0	0	0	0	0
	4	0	0	0	0	0	0	0	0	0	0	0	0
P3 (2 d)	0	1/3	3/3	3/3	0	3/3	3/3	1/2	0	0	0	4/4	3/4
	1	2/3	0	0	1/3	0	0	1/2	2/2	2/2	4/4	0	1/4
	2	0	0	0	1/3	0	0	0	0	0	0	0	0
	3	0	0	0	0	0	0	0	0	0	0	0	0
	4	0	0	0	1/3	0	0	0	0	0	0	0	0
P4 (3 d)	0	1/3	2/3	2/3	3/8	8/8	8/8	3/90	4/9	9/9	0	0	3/8
	1	1/3	0	1/3	3/8	0	0	5/90	5/9	0	5/8	4/8	2/8
	2	1/3	1/3	0	1/8	0	0	1/9	0	0	3/8	2/8	3/8
	3	0	0	0	1/8	0	0	0	0	0	0	2/8	0
	4	0	0	0	0	0	0	0	0	0	0	0	0

[a]Saccular-to-alveolar stage transition status of developing lungs.
[b]Numbers indicate fraction of the corresponding animal tissue sections to the total animal tissue sections in the study group used for microscopic evaluation of histopathology (one tissue slide per mouse). Each microscopic slide includes proximal (G5) and distal (G11) lung sections stained with hematoxylin and eosin.
[c]Airway lesions were evaluated by the severity of interstitial inflammation (II), alveolar edema (AE), and alveolar inflammation (AI). Score 1 is for minimal, 2 for mild, 3 for moderate, and 4 for marked injury.

did not cause significant lung injury in either of the genotypes, all further studies were performed with 100% O_2.

TGF-β, VEGF, and ANGPT2 protein expression. Protein concentrations of TGF-β associated with neonatal hyperoxia-induced lung injury were greater in *Nrf2*$^{-/-}$ relative to *Nrf2*$^{+/+}$ neonates at baseline and after hyperoxia (Fig. 3G). Basal levels of the angiogenesis factors VEGF and angiopoietin-2 (ANGPT2) were slightly lower in *Nrf2*$^{-/-}$ mice than in *Nrf2*$^{+/+}$ mice. Hyperoxia-increased VEGF levels at 3 days were higher in *Nrf2*$^{+/+}$ neonates relative to *Nrf2*$^{-/-}$ neonates (Fig. 3G). ANGPT2 was increased by O_2 (1–3 days) in *Nrf2*$^{+/+}$ but not in *Nrf2*$^{-/-}$ mice (Fig. 3G).

Pulmonary Nrf2 activation and oxidative stress after hyperoxia

Hyperoxia increased mRNA expression, nuclear translocation, and total ARE binding activity of pulmonary Nrf2 over the age-matched constitutive levels in *Nrf2*$^{+/+}$ neonates after 2 and 3 days (Fig. 4A). Total glutathione (GSH) level was significantly lower in *Nrf2*$^{-/-}$ compared with *Nrf2*$^{+/+}$ neonates at baseline and after 2–3 days of O_2 exposure (Fig. 4B). Hyperoxia significantly increased GSH in *Nrf2*$^{+/+}$ (1–3 days) and *Nrf2*$^{-/-}$ mice (1–2 days), but the induced GSH level was significantly lower in *Nrf2*$^{-/-}$ than in *Nrf2*$^{+/+}$ mice throughout exposure (Fig. 4B). At P4, significantly higher levels of baseline oxidized lipid (malondialdehyde [MDA]) were found in the lungs from *Nrf2*$^{-/-}$ relative to *Nrf2*$^{+/+}$ neonates (Fig. 4C). Hyperoxia (3 days) caused significantly higher increases of MDA in *Nrf2*$^{-/-}$ than in *Nrf2*$^{+/+}$ mice (Fig. 4C). Basal level of oxidatively modified proteins was higher in *Nrf2*$^{-/-}$ than in *Nrf2*$^{+/+}$ neonates at all times (Fig. 4D). Protein oxidation band intensity was elevated over baseline after 2 and 3 days of O_2 in *Nrf2*$^{-/-}$ lungs, and enhanced protein oxidation levels were markedly higher than those in *Nrf2*$^{+/+}$ lungs (Fig. 4D).

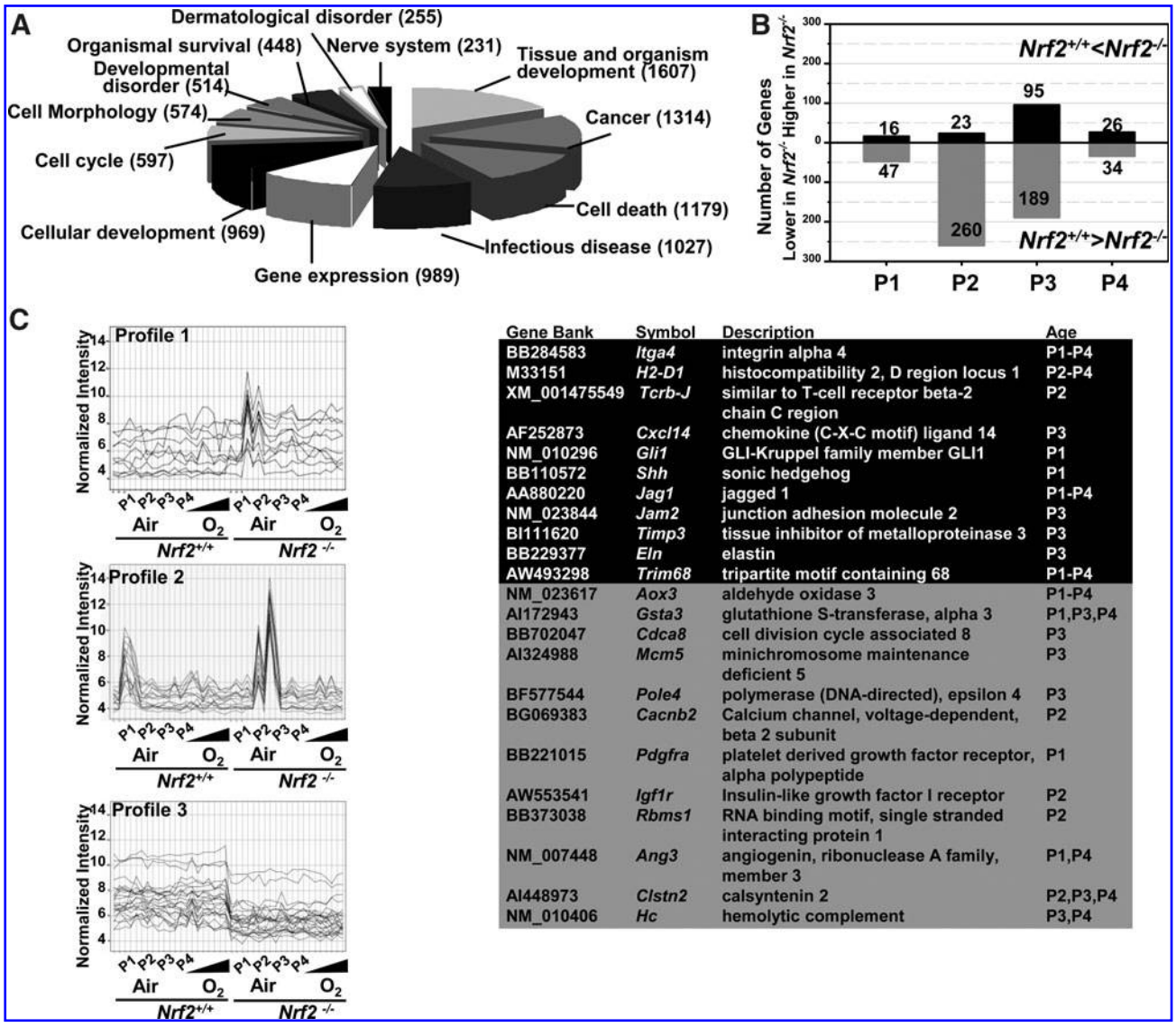

Gene Bank	Symbol	Description	Age
BB284583	*Itga4*	integrin alpha 4	P1-P4
M33151	*H2-D1*	histocompatibility 2, D region locus 1	P2-P4
XM_001475549	*Tcrb-J*	similar to T-cell receptor beta-2 chain C region	P2
AF252873	*Cxcl14*	chemokine (C-X-C motif) ligand 14	P3
NM_010296	*Gli1*	GLI-Kruppel family member GLI1	P1
BB110572	*Shh*	sonic hedgehog	P1
AA880220	*Jag1*	jagged 1	P1-P4
NM_023844	*Jam2*	junction adhesion molecule 2	P3
BI111620	*Timp3*	tissue inhibitor of metalloproteinase 3	P3
BB229377	*Eln*	elastin	P3
AW493298	*Trim68*	tripartite motif containing 68	P1-P4
NM_023617	*Aox3*	aldehyde oxidase 3	P1-P4
AI172943	*Gsta3*	glutathione S-transferase, alpha 3	P1,P3,P4
BB702047	*Cdca8*	cell division cycle associated 8	P3
AI324988	*Mcm5*	minichromosome maintenance deficient 5	P3
BF577544	*Pole4*	polymerase (DNA-directed), epsilon 4	P3
BG069383	*Cacnb2*	Calcium channel, voltage-dependent, beta 2 subunit	P2
BB221015	*Pdgfra*	platelet derived growth factor receptor, alpha polypeptide	P1
AW553541	*Igf1r*	Insulin-like growth factor I receptor	P2
BB373038	*Rbms1*	RNA binding motif, single stranded interacting protein 1	P2
NM_007448	*Ang3*	angiogenin, ribonuclease A family, member 3	P1,P4
AI448973	*Clstn2*	calsyntenin 2	P2,P3,P4
NM_010406	*Hc*	hemolytic complement	P3,P4

FIG. 2. Effect of *Nrf2* deletion on transcriptome of late saccular phase lungs. (A) Biological functions and disorders of 9737 Nrf2-dependent transcripts ($p < 0.05$) altered during postnatal ages P1–P4 were identified by ingenuity pathway analysis (IPA) and the number of genes in each function and disorder are depicted in a pie chart. **(B)** The number of transcripts significantly different (≥2-fold, $p < 0.01$) between $Nrf2^{+/+}$ and $Nrf2^{-/-}$ neonates at each postnatal day. Selected lung genes overexpressed (*black*) or suppressed (*gray*) in $Nrf2^{-/-}$ relative to $Nrf2^{+/+}$ neonates (from Supplementary Tables S2a, b) are presented. **(C)** Visual data profiling analysis (Spotfire) classified Nrf2-dependent profile patterns during P1–P4 (gene list in Supplementary Table S3). Signal intensity of individual sample transcript (each *vertical line*) is indicated as log2-normalized value.

Transcripomics during the development of hyperoxia-induced lung injury and the role of Nrf2

Lung genes modulated by hyperoxia in *Nrf2*$^{+/+}$ neonates. Transcripts upregulated by hyperoxia were enhanced mostly from 2 days and remained elevated, and they encoded antioxidant defense proteins, DNA damage/repair and apoptosis proteins, AP-1 family and other transcription factors, multiple chemokines and cytokines, cell adhesion/migration molecules, and organ development and angiogenesis factors (Supplementary Table S4A). Conversely, hyperoxia downregulated transcripts most predominantly at day 3. Affected genes encoded signal transducers of canonical pathways including cytochrome P450-mediated xenobiotic metabolism, lipid and hormone metabolism, molecule transport, and humoral immunity (Supplementary Table S4B). Overall, genes significantly modulated during the development of hyperoxia-induced injury ($n = 8529$, $p < 0.01$) have roles in cell cycle, tissue development, gene expression, lipid metabolism, cell–cell interaction, and immune response networks (Supplementary Table S4c).

Genes differentially modulated by hyperoxia in Nrf2$^{+/+}$ and *Nrf2*$^{-/-}$ neonates. During hyperoxia (1–3 days), 437 transcripts were significantly ($p < 0.01$) and differentially (≥2-fold) modulated between $Nrf2^{+/+}$ and $Nrf2^{-/-}$ neonates. k-Means clustering analysis determined genes that are

relatively suppressed in *Nrf2*$^{-/-}$ compared with *Nrf2*$^{+/+}$ neonates after hyperoxia (Fig. 5A sets 2, 4, and 5; Supplementary Table S5). They encoded proteins for gene expression machinery and cell growth (DNA replication/repair, apoptosis, transcription, translation, and cell cycle) and redox homeostasis including multiple ARE-responsive antioxidant/defense genes. Conversely, gene transcripts with higher expression in *Nrf2*$^{-/-}$ lungs were involved in endocytosis, transport, and development (Fig. 5A sets 1 and 3; Supplementary Table S5). These Nrf2-dependent genes have functions in cancer, cell growth and development, lipid metabolism, and small molecule biochemistry during the development of hyperoxic lung injury (Fig. 5B). Canonical pathway (Supplementary Table S5) and functional network (Supplementary Fig. S2) analyses depicted time-dependent events modulated by Nrf2 during the pathogenesis, which were acute-phase organ injury (1 day), organ morphology (1–2 days), cell growth and proliferation (2 days), vasculature development (2 days), immune response (2–3 days), TGF-β signaling (3 days), hematological system development and function (3 days), and cell–cell interaction and signaling (3 days). Visual data mining (Fig. 5C and Supplementary Table S3) determined a unique profile of Nrf2-dependent genes suppressed basally and did not respond to hyperoxia in *Nrf2*$^{-/-}$ mice (profile 4; *e.g.*, *Gpx2*, *Txnrd1*, and *Creg1*) while several genes (*e.g.*, *Mtr*, *Sbf2*, and MHCII) were markedly overexpressed at P2–P3 and were relatively decreased by O_2 only in *Nrf2*$^{-/-}$ mice (profile 5).

Because many genes associated with DNA replication/repair and redox homeostasis were relatively suppressed in *Nrf2*$^{-/-}$ neonates during hyperoxia, DNA damage and protein levels of a DNA replication and cell proliferation marker PCNA were compared in *Nrf2*$^{-/-}$ and *Nrf2*$^{+/+}$ lungs. Significant increases in genomic (1 and 3 days) and mitochondrial (1 and 2 days) DNA base lesions were found only in *Nrf2*$^{-/-}$ neonates exposed to 100% O_2 (Fig. 5D). In addition to postnatal age-dependent increase (Fig. 1D), hyperoxia-induced increase of nuclear PCNA was marked at 2 days in both genotypes, relative to corresponding air controls (Fig. 5D). However, the hyperoxia-induced level as well as basal abundance at 1–2 days (P2–P3) were relatively lower in *Nrf2*$^{-/-}$ neonates compared with *Nrf2*$^{+/+}$ neonates.

Validation of microarray gene expression profiles and functional relevance

Nrf2-dependent lung expression profiles. Quantitative reverse transcription–polymerase chain reaction (qRT-PCR) analysis (Fig. 6A, left) and western blot analysis (Fig. 6A, right) confirmed microarray expression profiles of selected transcripts or their protein products, including histocompatibility 2 (*H2-Q1*, *H2-D1*, and H2-Ea), *Inta4*, *Nqo1*, *Akr1b8*, *Hc*, *Aox1*, *Jag1*, *Rad51*, and *Egr2*, which varied between *Nrf2*$^{+/+}$ and *Nrf2*$^{-/-}$ neonates during P1–P4. Message profiles of selected hyperoxia-responsive, Nrf2-dependent genes *Akr1b8*, *Clstn2*, *Nqo1*, *Hc*, *Ang3*, *Slc7a11*, *Gpx2*, GCS (for *Gclc*), GST-μ (for *Gstm*), HO-1 (for *Hmox1*), and MARCO determined by qRT-PCR (Fig. 6B, left) or western blotting (Fig. 6B, right) were also consistent with those observed by microarray analysis.

Putative AREs in the promoter of potential Nrf2 effector genes. Putative ARE or ARE-like sequences were analyzed in 5-kb upstream sequences of selected genes regulated in an Nrf2-dependent manner to evaluate their potential as direct Nrf2 effectors using a position weight matrix (PWM) statistical model (48). A majority of the listed genes in Table 2 (a selected binding motif from each representative gene presented) had multiple ARE-like binding sequences, and their PWM scores and matrix similarity score were as high as those of the validated AREs in Nrf2 target genes (*e.g.*, *Txnrd1* and *Ftl*). Importantly, many of these target genes containing potential AREs were also identified as Nrf2 effectors by chromatin immunoprecipitation sequencing performed in human (8) and/or mouse cells (30), thus supporting their functional roles. Taken together, results strongly suggest a role for Nrf2 through binding to these genes in modulation of angiogenesis, cell cycle, tissue development, and cell-to-cell interaction in newborn lungs and during injury pathogenesis.

Functional role of Nrf2 downstream effectors: glutathione peroxidase 2 and macrophage receptor with collagenous structure. ARE-bearing macrophage receptor with collagenous structure (*Marco*) and glutathione peroxidase 2 (*Gpx2*) were identified as key Nrf2 downstream effectors in the

FIG. 3. Enhanced susceptibility of *Nrf2*$^{-/-}$ neonates to hyperoxia. Significantly increased hyperoxia susceptibility of newborn *Nrf2*$^{-/-}$ mice relative to *Nrf2*$^{+/+}$ newborns was determined by lower body weight gain after 3 days of 100% O_2 or after 6 days of 70% O_2 **(A)**; more severe mortality after 1–5 days of 100% O_2 exposure **(B)**; enhanced total protein concentration, and the number of neutrophils and monocytes in bronchoalveolar lavage (BAL) fluids at 3 days after 100% O_2 **(C)**; and heightened necrotic and apoptotic airway cell death after 3 days of 100% O_2 **(D)**. All data are presented as mean ± standard error of the mean (SEM). *Significantly different from genotype-matched air controls ($p < 0.05$). +Significantly different from exposure-matched *Nrf2*$^{+/+}$ mice ($p < 0.05$). $n = 5$–17/group for mean % body weight data. $n = 10$–12 for 2 days and $n = 22$–39 for 3–5 days mortality data. $n = 6$/group for BAL data. Necrotic lung cell death was quantified in aliquots of BAL using a colorimetric lactate dehydrogenase (LDH) assay ($n = 6$/group). Airway cell apoptosis was determined by deoxynucleotidyl transferase-mediated dUTP nick-end labeling (TUNEL) and National Institutes of Health (NIH) Image analysis ($n = 3$/group). TUNEL-stained lung cells were barely detected in air controls of either genotype. **(E)** Representative Giemsa-stained cytocentrifuged BAL fluid cells indicate markedly greater lung cell death (*arrows*) by lysis or apoptosis and airway neutrophilic infiltration (*arrow heads*) in *Nrf2*$^{-/-}$ than in *Nrf2*$^{+/+}$ mice after 3 days of 100% O_2. Bars = 50 μm. **(F)** Augmented adverse lung histopathology in *Nrf2*$^{-/-}$ neonates relative to *Nrf2*$^{+/+}$ after hyperoxia indicated by greater pulmonary epithelial thickening, perivascular-peribronchiolar edema, and protein exudates in air space (*arrows*) after 3 days of 100% O_2. Representative light photomicrographs of hematoxylin and eosin (H&E)-stained lung tissue sections are presented ($n = 3$–9/group). Bars = 100 μm. **(G)** Differential protein expression of transforming growth factor beta (TGF-β), and angiogenesis factors for lung development, vascular endothelial growth factor (VEGF), and angiopoietin 2 (ANGPT2), between *Nrf2*$^{+/+}$ and *Nrf2*$^{-/-}$ neonates basally and after O_2. Representative band images of multiple applications are shown ($n = 3$/group). (To see this illustration in color the reader is referred to the web version of this article at www.liebertonline.com/ars)

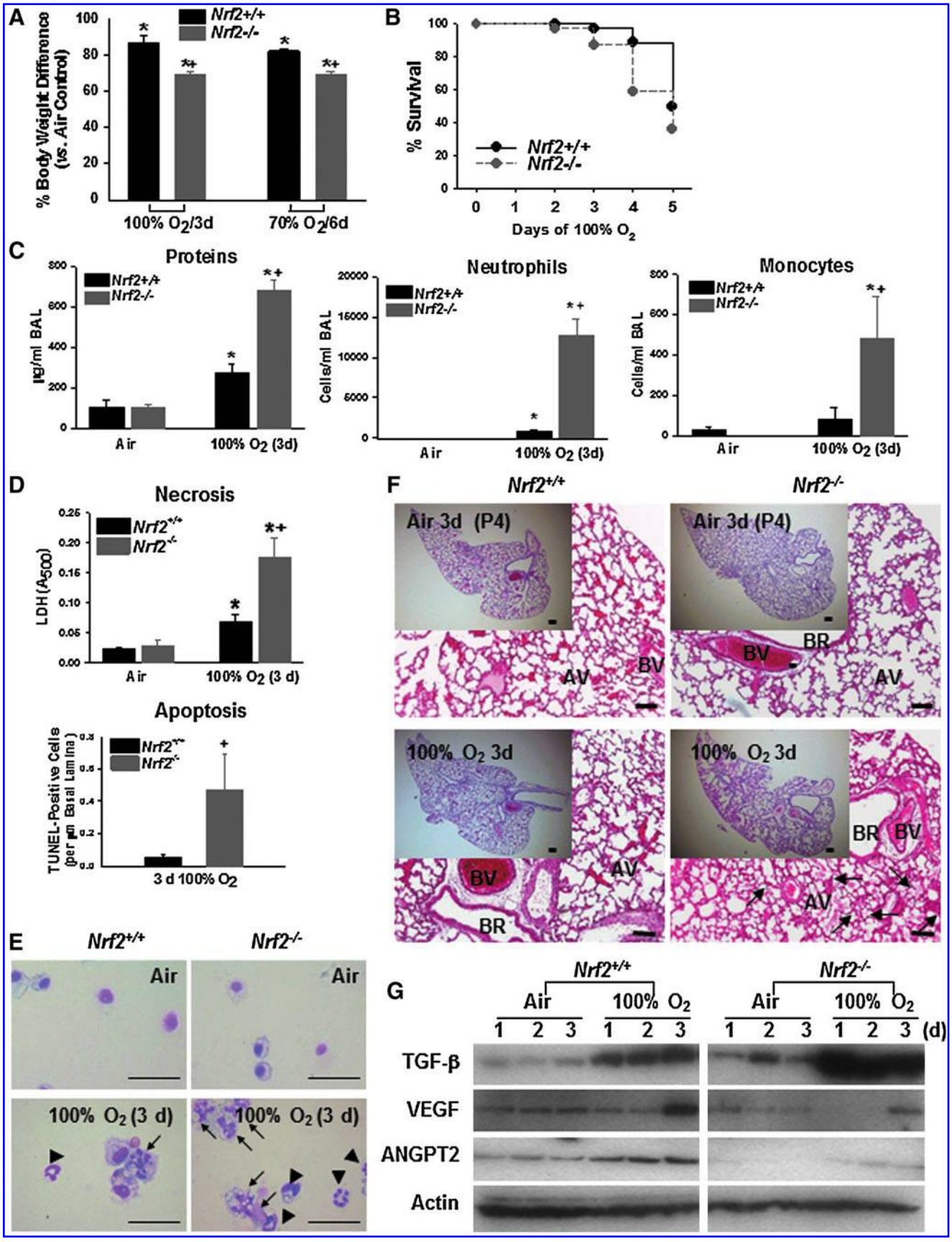
A
% Body Weight Difference (vs. Air Control)
Nrf2+/+
Nrf2-/-
100% O2/3d
70% O2/6d
B
% Survival
Nrf2+/+
Nrf2-/-
Days of 100% O2
C
Proteins
μg/ml BAL
Neutrophils
Cells/ml BAL
Monocytes
Cells/ml BAL
Air
100% O2 (3d)
D
Necrosis
LDH (A500)
Apoptosis
TUNEL-Positive Cells (per μm Basal Lamina)
3 d 100% O2
E
Nrf2+/+
Nrf2-/-
Air
100% O2 (3 d)
F
Nrf2+/+
Nrf2-/-
Air 3d (P4)
100% O2 3d
BV
AV
BR
G
Nrf2+/+
Nrf2-/-
Air
100% O2
1 2 3 1 2 3 (d)
TGF-β
VEGF
ANGPT2
Actin

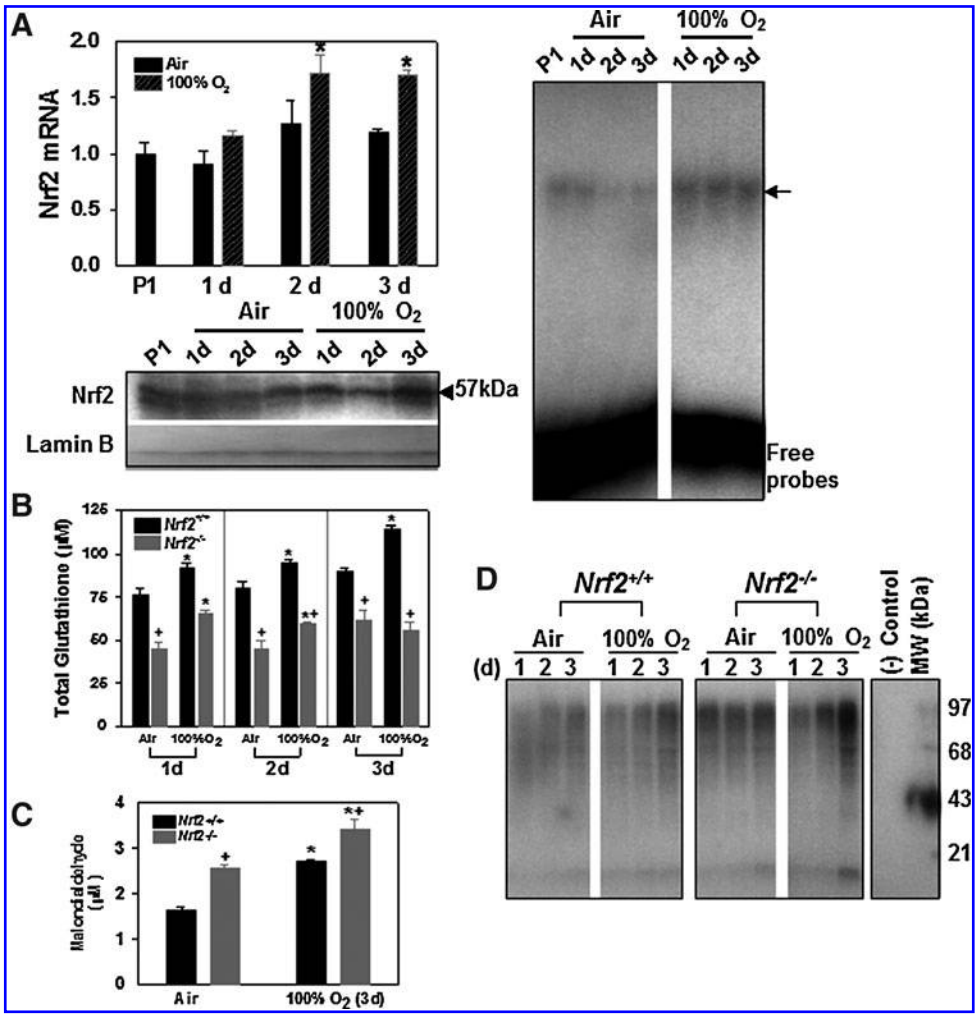

FIG. 4. Lung Nrf2 activation and redox status after hyperoxia. (A) Hyperoxia increased Nrf2 message as determined by semi-quantitative reverse transcription–polymerase chain reaction (RT-PCR) in $Nrf2^{+/+}$ mice after 2–3 days of 100% O_2, while basal level of Nrf2 mRNA did not vary significantly between ages P1 and P4. Data presented as mean ± SEM ($n = 3$/group) after normalization to the level at P1. *Significantly different from time-matched air controls ($p < 0.05$). Nuclear translocation of Nrf2 determined by Western blot analysis of lung nuclear protein aliquots (20 μg) was enhanced by 1–3 days of 100% O_2 over the corresponding air controls in $Nrf2^{+/+}$ mice. Nuclear lamin B level was determined as a loading control. Gel shift analysis demonstrated enhanced total antioxidant response element (ARE) binding activity of lung nuclear proteins at 1–3 days of O_2 relative to time-matched air controls in $Nrf2^{+/+}$ mice. *Arrow* indicates shifted bands for nuclear protein (5 μg) bound to ARE consensus sequence. Representative digitized bands from duplicate Western blotting and gel shift analysis are presented. **(B)** Reduced lung glutathione in $Nrf2^{-/-}$ mice compared with $Nrf2^{+/+}$ mice at baseline and after hyperoxia. Mean ± SEM presented ($n = 3$/group). *Significantly different from genotype-matched air control mice ($p < 0.05$). +Significantly lower than exposure-matched $Nrf2^{+/+}$ mice ($p < 0.05$). **(C)** Different levels of lung lipid peroxidation evaluated by malondialdehyde (MDA) level in BAL from $Nrf2^{+/+}$ and $Nrf2^{-/-}$ neonates after 3 days air and O_2. Mean ± SEM ($n = 4$/group) is presented. *Significantly different from genotype-matched air control mice ($p < 0.05$). +Significantly different from O_2-exposed $Nrf2^{+/+}$ neonates ($p < 0.05$). **(D)** Heightened oxidized proteins in $Nrf2^{-/-}$ neonates determined by immunoblotting analysis of carbonyl moieties detected in 30–100 kDa lung proteins after 3 days of air or O_2. (−) control, nonderivatized protein samples. MW, protein molecular weight marker.

current model as they were distinctly suppressed in $Nrf2^{-/-}$ neonates at P1–P4, and were highly induced during exposure to O_2. Lung injury responses to hyperoxia in $Marco^{-/-}$ and $Gpx2^{-/-}$ neonates were compared with their wild-type controls. Significantly greater numbers of BAL neutrophils were found in $Marco^{-/-}$ and $Gpx2^{-/-}$ mice compared with respective wild-type mice after 3 days of O_2, and the number of BAL macrophages after O_2 was also significantly greater in $Marco^{-/-}$ than in $Marco^{+/+}$ neonates (Fig. 6C, D). Overall, data indicate functional roles for *Marco* and *Gpx2* in hyperoxia-induced lung inflammation.

Discussion

While Nrf2 is a critical modulator for protection against a broad range of oxidative disorders in adults, its role in tissue development or the pathogenesis of neonatal or childhood disease has received little attention. In the current study,

transcriptomic analysis indicated that Nrf2 is critical to processes/networks for cell cycle and DNA repair, immune function, morphogenesis and lung development, and antioxidant defense during postnatal normal lung maturation in mice. Importantly, we found a beneficial role for Nrf2 in hyperoxia-induced injury of undeveloped lung. *Nrf2* is a susceptibility gene for protection against acute lung injury caused by 100% O_2 in adult mice (13, 14, 38). Our results demonstrate Nrf2-dependent alleviation of hyperoxia-induced injury phenotypes in the saccular phase of lung, including arrest in alveolar development evidenced by lower RAC and reduced appearance of multilobular alveoli/branched septi as well as severe exudative-phase diffuse alveolar damage characterized by edema, leukocyte inflammation, and cell death in $Nrf2^{-/-}$ mice. Moreover, highly suppressed GSH pools as well as heightened pulmonary oxidation and DNA lesions in $Nrf2^{-/-}$ neonates indicated the critical roles for ROS and Nrf2-directed defense in the pathogenesis of hyperoxia-induced lung injury. The current study warrants further investigation of Nrf2 in other oxidant-associated lung disease models at early ages. Juvenile $Nrf2^{-/-}$ mice that were exposed to hyperoxia as neonates had more severely hindered resolution of lung damage relative to juvenile $Nrf2^{+/+}$ mice that were similarly exposed as neonates (31). This observation supported an association of the severity of hyperoxia-induced injury in infancy with persisting or long-term pulmonary outcome. It also suggests the potential for exacerbation of oxidative pulmonary disease in adults or adolescents who had BPD in infancy.

The current study initially characterized complex gene expression networks in the saccular stage during postnatal lung maturation. Variation in lung gene expression was greatest at P1 relative to age P4, likely reflecting the influence of direct contact of airway cells to the extra-uterine environment. Importantly, *Nrf2* significantly modulated genes involved not only in redox balance but also in tissue and organ development, cancer, cell death, and infectious disease during saccular-to-alveolar transition. The marked overexpression of multiple major histocompatibility complex, class II (MHCII), lymphatic system, and cell–cell interaction genes (*e.g.*, *Itga4* and *Cxcl14*) in naive lungs from $Nrf2^{-/-}$ neonates suggested their aberrant basal immunity as evidence by enhanced susceptibility of adult $Nrf2^{-/-}$ mice to asthma and allergy (28, 37).

Our microarray analysis also evaluated Nrf2-dependent antioxidant capacity under normoxic and hyperoxic conditions in the immature lungs. Direct antioxidants, including superoxide dismutases (SODs), are known to be highly activated in the lung shortly after birth (34), and we found that all the redox genes that varied during P1–P4 were higher at P1 relative to P2–P4. *In utero* expression of airway antioxidant enzymes is known to increase toward term gestation to prepare for birth into an O_2-rich (from 3% to 21%) environment (39). Therefore, preterm infants with low birth weight are not only more sensitive to increased O_2 concentrations compared with adults (10), but they also have diminished/compromised endogenous antioxidant activity relative to full-term infants (39), which contributes to the critical consequence of hyperoxic insult in BPD pathogenesis. However, overall clinical results from therapies with antioxidants (*e.g.*, SODs, vitamins A and E, N-acetylcysteine, and metalloporphyrin) have remained inconclusive in preterm infants (1, 45). In the current study, we identified novel antioxidants (*e.g.*, *Akr1b8*, *Cbr2*, *Pgd*, and *Slc7a11*) that were induced during the development of neonatal hyperoxic injury, but not in lungs of adult mice exposed to hyperoxia (15). These gene products have roles in redox balance through a broad spectrum of pathways, including metabolic process, small molecular biochemistry, and membrane transport. Importantly, *Slc7a11* [solute carrier family 7 (cationic amino acid transporter, y^+ system), member 11] encodes xCT that is a key component of high-affinity cysteine/glutamate exchange transporter system χ_c^-, which mediates cellular cystine uptake for GSH synthesis (41). Identification of putative AREs in these Nrf2 effectors suggests their therapeutic potentials in preventing oxidant-induced injury in the neonate lung.

Neonatal pulmonary oxidative stress was obvious after hyperoxia exposure regardless of genotypes, while *Nrf2* deficiency elevated oxidative proteins and lipid peroxidation at baseline as well as after hyperoxia. Although widely used, the amount of MDA as a lipid peroxidation marker is known to be affected by several variables (22). It would be worth validating the effect of *Nrf2* deletion on oxidant tissue injury by measurement of a more reliable lipid peroxidation marker 8-*iso*-Prostaglandin F2α (32). Importantly, oxidative DNA damage is considered a causative factor in diverse pulmonary disorders, including neoplasia and acute lung injury. Previous studies have shown that hyperoxia caused base adduct formation (*e.g.*, 7,8-dihydro-8-oxo-guanine) and DNA strand breakage in lungs of adult mice (4); DNA adduct formation was found in most lung cells after the exposure, while the

FIG. 5. Effect of *Nrf2* deletion on lung transcriptome during pathogenesis of hyperoxia-induced lung injury. (A) Nrf2-dependently changed genes during hyperoxia ($n = 437$, $p < 0.01$) were grouped into 5 *k*-means cluster profiles (GeneSpring). Transcript expression is indicated as relative log ratio after normalization to time-matched $Nrf2^{+/+}$ air control. Selected genes from each cluster are listed. **(B)** Nrf2-dependent genes modulated by hyperoxia on each day were classified into biological functions and disorders by IPA, and plotted against the number of genes associated. **(C)** Visual profiling analysis (Spotfire) clustered several distinct genes showing unique Nrf2-dependent expression pattern during hyperoxia exposure. Profile 4 includes thioredoxin reductase 1 (*Txnrd1*) and cellular repressor of E1A-stimulated genes 1 (*Creg1*). Profile 5 includes major histocompatibility complex, class II genes (*e.g.*, *H2-Ea*) and 5-methyltetrahydrofolate-homocysteine methyltransferase (*Mtr*). Signal intensity of individual sample transcript (each *vertical line*) is indicated as log2-normalized value. **(D)** Lesion frequencies in genomic (DNA polymerase β gene) and mitochondrial DNA were compared in $Nrf2^{+/+}$ and $Nrf2^{-/-}$ mice after air or hyperoxia (100%). All data were normalized to 1 day air-exposed $Nrf2^{+/+}$ mice and group mean ± SEM is presented ($n = 3$/group). Background noise level (*dashed lines*) is set at ± 0.15. *Significantly different from genotype- and time-matched air controls ($p < 0.05$). +Significantly different from exposure- and time-matched $Nrf2^{+/+}$ mice ($p < 0.05$). PCNA level was determined as a marker for S-phase cells undergoing proliferation by Western blotting in nuclear extracts of $Nrf2^{+/+}$ and $Nrf2^{-/-}$ lungs. Nuclear lamin B level was determined as a loading control. Representative band images from replicates are shown.

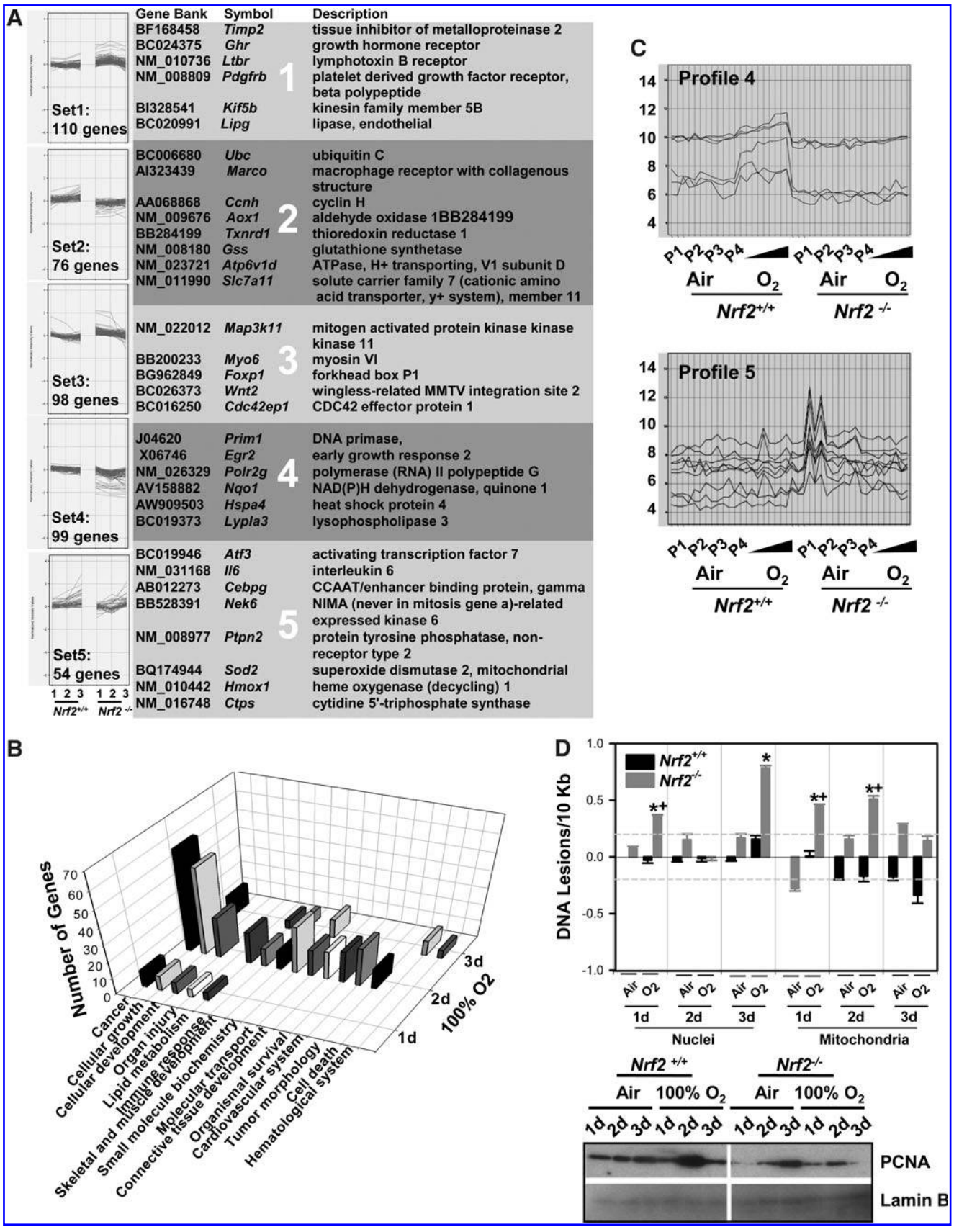
A
Gene Bank Symbol Description
Set1: 110 genes
BF168458 Timp2 tissue inhibitor of metalloproteinase 2
BC024375 Ghr growth hormone receptor
NM_010736 Ltbr lymphotoxin B receptor
NM_008809 Pdgfrb platelet derived growth factor receptor, beta polypeptide
BI328541 Kif5b kinesin family member 5B
BC020991 Lipg lipase, endothelial
1
Set2: 76 genes
BC006680 Ubc ubiquitin C
AI323439 Marco macrophage receptor with collagenous structure
AA068868 Ccnh cyclin H
NM_009676 Aox1 aldehyde oxidase 1BB284199
BB284199 Txnrd1 thioredoxin reductase 1
NM_008180 Gss glutathione synthetase
NM_023721 Atp6v1d ATPase, H+ transporting, V1 subunit D
NM_011990 Slc7a11 solute carrier family 7 (cationic amino acid transporter, y+ system), member 11
2
Set3: 98 genes
NM_022012 Map3k11 mitogen activated protein kinase kinase kinase 11
BB200233 Myo6 myosin VI
BG962849 Foxp1 forkhead box P1
BC026373 Wnt2 wingless-related MMTV integration site 2
BC016250 Cdc42ep1 CDC42 effector protein 1
3
Set4: 99 genes
J04620 Prim1 DNA primase,
X06746 Egr2 early growth response 2
NM_026329 Polr2g polymerase (RNA) II polypeptide G
AV158882 Nqo1 NAD(P)H dehydrogenase, quinone 1
AW909503 Hspa4 heat shock protein 4
BC019373 Lypla3 lysophospholipase 3
4
Set5: 54 genes
BC019946 Atf3 activating transcription factor 7
NM_031168 Il6 interleukin 6
AB012273 Cebpg CCAAT/enhancer binding protein, gamma
BB528391 Nek6 NIMA (never in mitosis gene a)-related expressed kinase 6
NM_008977 Ptpn2 protein tyrosine phosphatase, non-receptor type 2
BQ174944 Sod2 superoxide dismutase 2, mitochondrial
NM_010442 Hmox1 heme oxygenase (decycling) 1
NM_016748 Ctps cytidine 5'-triphosphate synthase
5
1 2 3 1 2 3
Nrf2+/+ Nrf2 -/-
C
Profile 4
14 12 10 8 6 4
P1 P2 P3 P4 P1 P2 P3 P4
Air O2 Air O2
Nrf2+/+ Nrf2 -/-
Profile 5
14 12 10 8 6 4
P1 P2 P3 P4 P1 P2 P3 P4
Air O2 Air O2
Nrf2+/+ Nrf2 -/-
B
Number of Genes
70 60 50 40 30 20 10 0
Cancer
Cellular growth
Cellular development
Organ injury
Lipid metabolism
Immune response
Skeletal and muscle development
Small molecule biochemistry
Molecular transport
Connective tissue development
Organismal survival
Cardiovascular system
Tumor morphology
Cell death
Hematological system
1d
2d
3d
100% O2
D
DNA Lesions/10 Kb
1.0 0.5 0.0 -0.5 -1.0
Nrf2+/+
Nrf2-/-
*+
*
*+
*+
Air O2 Air O2 Air O2 Air O2 Air O2 Air O2
1d 2d 3d 1d 2d 3d
Nuclei Mitochondria
Nrf2 +/+ Nrf2-/-
Air 100% O2 Air 100% O2
1d 2d 3d 1d 2d 3d 1d 2d 3d 1d 2d 3d
PCNA
Lamin B

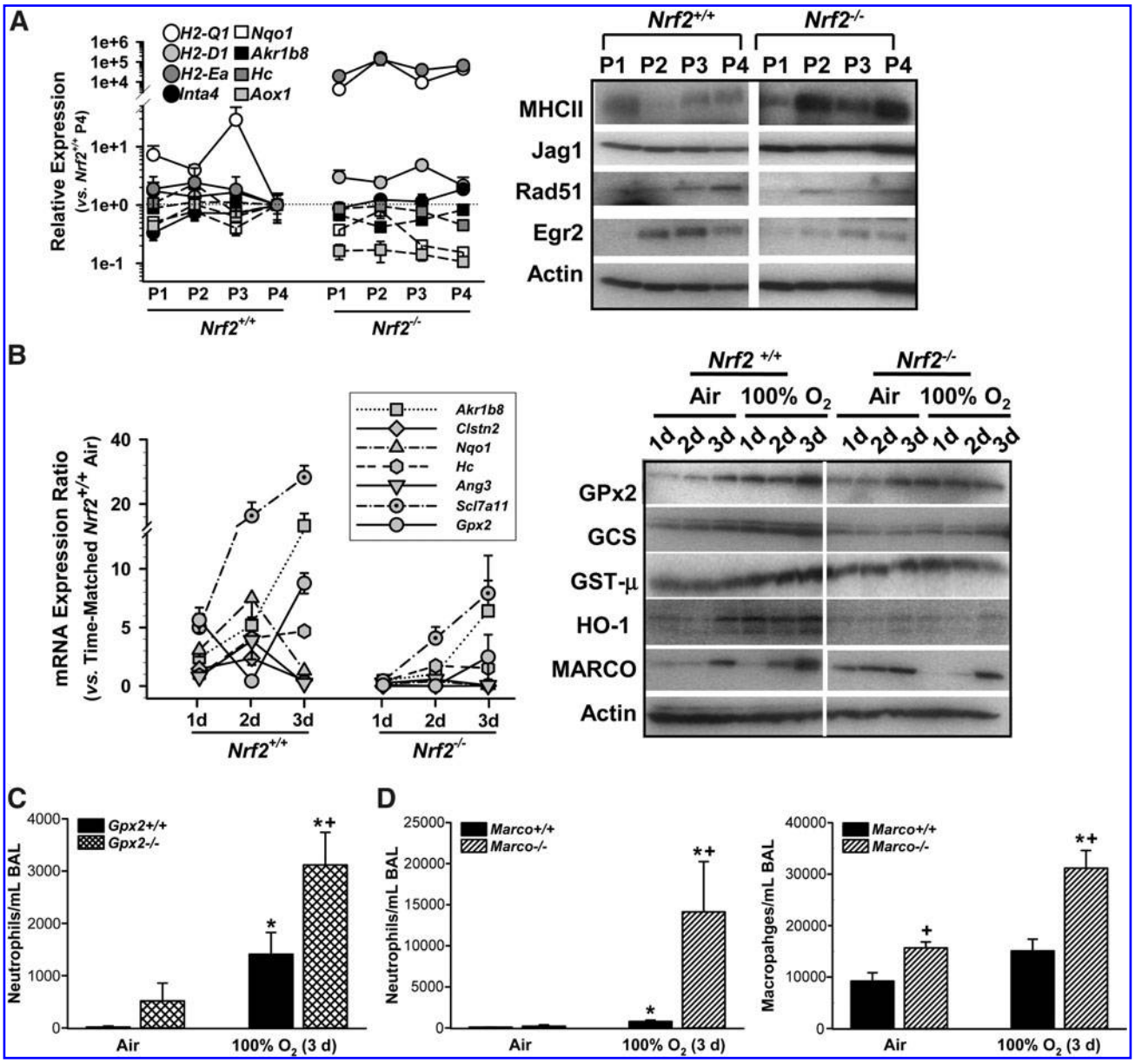

FIG. 6. Validation of microarray profiles and role for Nrf2 effectors in hyperoxia-induced lung injury pathogenesis. Selected transcripts differentially expressed between $Nrf2^{+/+}$ and $Nrf2^{-/-}$ neonates at P1–P4 **(A)** and during hyperoxia exposure **(B)** were confirmed by quantitative (q)RT-PCR and/or Western blot analyses. qRT-PCR graphs present fold differences of each gene expression relative to P4 level in $Nrf2^{+/+}$ after normalization to corresponding 18s expression **(A)** or depict fold differences relative to time-matched $Nrf2^{+/+}$ air control of 18s-normalized data **(B)**. Group mean ± SEM is presented ($n = 3$/group). Actin level was determined as internal control for western blotting. Representative digitized bands from multiple blot analysis are presented. *H2-Q1*, histocompatibility 2, Q region locus 1; *H2-D1*, histocompatibility 2, D region locus 1; *Inta4*, integrin alpha 4; *Nqo1*, NAD(P)H:quinone oxidoreductase 1; *Akr1b8*, aldo-keto reductase family 1, member B8; *Hc*, hemolytic complement; *Aox1*, aldehyde oxidase 1; *Jag1*, jagged 1; *Rad51*, RAD51 homolog; *Egr2*, early growth response 2; *Clstn2*, calsyntenin 2; *Ang3*, angiogenin, ribonuclease A family, member 3; *Slc7a11*, solute carrier family 7, member 11; *Gpx2*, glutathione peroxidase 2; *Gclc* or GCS, glutamate cysteine ligase, catalytic subunit; *Gstm* or GST-μ, glutathione S-transferase M; *Ho1*, heme oxygenase-1; *Marco*, macrophage receptor with collagenous structure. Functional roles of ARE-bearing *Gpx2* **(C)** and *Marco* **(D)** in hyperoxia-induced lung inflammation were determined by BAL analysis in gene-targeted neonates after 100% of O_2 (3 days). Mean ± SEM ($n = 4$/group) is presented. *Significantly different from genotype-matched air control ($p < 0.05$). +Significantly different from exposure-matched wild-type controls ($p < 0.05$).

most severe level of damage, phosphodiester backbone breakage, was found only in type 2 cells, which resulted in the cell death and was associated with lung injury. Consistent with Nrf2-dependent variation in pulmonary apoptotic cell death and DNA lesions, microarray analysis also identified Nrf2-dependent dysregulation of genes involved in the DNA damage/repair and methylation pathways under conditions of normoxia (*e.g.*, *Rad51* and *Chek1*) and hyperoxia (*e.g.*, *Rbm14* and *Mtrr*). In particular, significant suppression of mitochondrial superoxide dismutase (*Sod2*; Supplementary

Table 2. Putative Antioxidant Response Elements Determined by Bioinformatics in 5 kb Upstream Promoter Sequences of Selected Genes

Murine chromosome	*Gene symbol*	*Search starts*	*Search ends*	*Distance to TSS*	ARE-like *Sequence*	*PWM score*	*MS score*	*ChIP-Seq peak*
1	*Aox1*	58086489	58086509	−324	gggaaGTGACTCAGCAgtaca (F)[a]	15	0.943	M
	Creg1	167693628	167693648	−283	gcactGTGACTTAGGAagttg (F)	13	0.836	M
	Ephx1	182951112	182951132	−3506	gatctTCCTGAGTCAGtgccc (R)	11.6	0.825	M
	Marco	122402581	122402601	−940	accctTTGAATCTGCAtttta (F)	8.9	0.828	ND
2	*Itga4*	79093695	79093715	−1889	catggTGCTTTGTCACagcaa (R)	12.8	0.899	ND
	Itga6	71621002	71621022	−4138	agaaaATGAAACAGCCccatg (F)	8.7	0.814	C
	Jag1	136943942	136943962	−1706	ccagtTGCAAACTCATtctga (R)	11.5	0.828	M
	Rad51	118934450	118934470	−4104	tgtggTGCTAATTCATgaagt (R)	9	0.846	ND
	Srxn1	151931209	151931229	−257	tcaccCTGAGTCAGCGgccgg (F)	12.7	0.862	M, C
3	*Slc7a11*	50247634	50247654	−99	ccaacATTACTCAGCTCtttt (F)	14.1	0.843	M, C
	Gstm1	107825209	107825229	−4338	ccagtCTGACTGGGCCcctat (F)	9.3	0.851	M
	Npnt	132617392	132617412	−4157	gagagATGACTCAGCAgttaa (F)	16.2	0.947	M
4	*Ccne2*	11117832	11117852	−670	gtgtgTGCCGTGTCACccgca (R)	12.2	0.869	ND
	Cdca8	124617315	124617335	−3174	tcaggCTTACACGGCAagtgc (F)	10.9	0.787	ND
	Pgd	148544961	148544981	−4165	tcacaTTGACTCAGCataatt (F)	18.6	0.971	M, C
	Prdx1	116358065	116358085	−139	gaaagCGCTGAGTCATccccc (R)	15.7	0.92	M, C
5	*Ubc*	125872181	125872201	−1814	agctgGTGACTCAGCCaagaa (F)	12.7	0.907	M
6	*Tnfrsf1a*	125299104	125299124	−637	ctcttTGCTATGTCAGggcag (R)	11.6	0.886	M, C
7	*Arrdc4*	75896461	75896481	−2357	ttaccTGCTGAGTCATctcac (R)	13.2	0.933	M
	Ftl	52716343	52716363	−1107	tcagcGTGACTCAGCAgaact (F)	20.7	0.981	M, C
8	*Hmox1*	77613643	77613663	−3874	gatttTGCTGAGTCACcctct (R)	19.3	0.968	M
	Nqo1	109927527	109927547	−442	tcacaGTGAGTCGGCAaaatt (F)	16.4	0.87	M, C
9	*Chordc1*	18092725	18092745	−3986	caattTTCTGTGTCACaggcc (R)	11	0.805	M
	Gclc	77598546	77598566	−3796	cagagTGCTGAGTCACggtga (R)	21.6	0.99	M,C
10	*Egr2*	66996796	66996816	−3822	ccaccCTGACAAGGCAttcct (F)	12.6	0.871	ND
	Txnrd1	82321853	82321873	−98	attttTGCTTTGTCATtctga (R)	17.9	0.928	M, C
11	*Cdc6*	98769345	98769365	−120	tctgaGGCTGGGTCAGggagg (R)	10.2	0.874	C
	Cltc	86572978	86572998	−2004	aaatcTGCTTAGTCATtttag (R)	15.2	0.935	M, C
12	*Entpd5*	85749904	85749924	55	gcgcgGTGAGTGTGCAcgagc (F)	8.8	0.813	M, C
	Gpx2	77899598	77899618	−3077	ttgttTGCTAAGTCAGggaga (R)	15.1	0.931	ND
13	*Tbce*	14136510	14136530	−4663	ctgaaGTGAAACAGCAaaaaa (F)	9.5	0.835	M
14	*Ang2*	51818765	51818785	−3187	tacttGGCCTAGTCATgctca (R)	13.1	0.868	ND
	Ang3	44533492	44533512	−1243	tcgaaATGAGCAAGCAaatat (F)	10.5	0.825	ND
	Ednrb	104247230	104247250	−4337	caccaGTGAGACAGCGtgaag (F)	8.9	0.812	M
16	*Cbr3*	93682727	93682747	−737	ggaaaCGCTGAATCACtgtga (R)	14.1	0.875	M
17	*H2-D1*	35397765	35397785	−2275	cctgcTGCTAGGTCAGgcttg (R)	11.7	0.887	C
	Pbx2	34727868	34727888	−1548	caccaTCCTTAGTCACcaggt (R)	9.1	0.807	C
	Socs5	87503882	87503902	−3137	ggcacTGCCGAGTAAGgagta (R)	8.3	0.787	M
19	*Ltbp3*	5739637	5739657	−1267	tgaacTACTGAGTCACctttc (R)	11.8	0.839	C
	Rbm4	4796950	4796970	−3093	acaggGTGAATGAGCAcgtga (F)	11.9	0.867	C

[a]Uppercase indicates ARE core-like sequences (5′-RTKAYnnnGCR-3′; R = A or G, K = G or T, Y = C or T, *n* = A, C, G, or T), forward (F) or reverse complementary (R).

ND, not detected; ARE, antioxidant response element; TSS, transcription start site; PWM, position weight matrix; MS score, matrix similarity score; ChIP-Seq, chromatin immunoprecipitation-sequencing; M, Malhotra *et al.* (2010) (30); C, Campbell *et al.* (2010) (8).

Table S4a) is likely to be a factor leading to increased mitochondrial damage in *Nrf2*$^{-/-}$ neonates. Although epigenetic effects of hyperoxia and *Nrf2* dependency were beyond the scope of the current analysis, evidence indicates that hyperoxia causes hypermethylation in CpG islands of a lung gene in rats (50). Further, hyperoxia-induced DNA damage influenced global DNA methylation status in lung epithelial cells (35).

Impaired pulmonary vasculature development in ventilated preterm infants is thought to be caused by complex interactions of lung immaturity and postnatal factors including O_2, which results in arrest of alveolar growth (42). Maturation of pulmonary vessel walls in BPD involves numerous growth components, including VEGF-A and ANGPTL2, and other factors, such as angiogenins and extracellular matrix proteins (42). In the current study, lung ANGPTL2 proteins and *Ang3* transcripts were suppressed in *Nrf2*$^{-/-}$ mice relative to *Nrf2*$^{+/+}$ mice constitutively and/or after hyperoxia, and 5′-flanking regions of *Ang2* and *Ang3* contained potential AREs. We speculate that although there was no effect on normal lung maturation, the differential constitutive levels of these proteins between two genotypes may predispose *Nrf2*$^{-/-}$ neonates to enhanced susceptibility to hyperoxia. Other multiple angiogenic or antiangiogenic genes (*e.g.*, *Agtrl1*, *Tie1*, *Eng*, *Il6*,

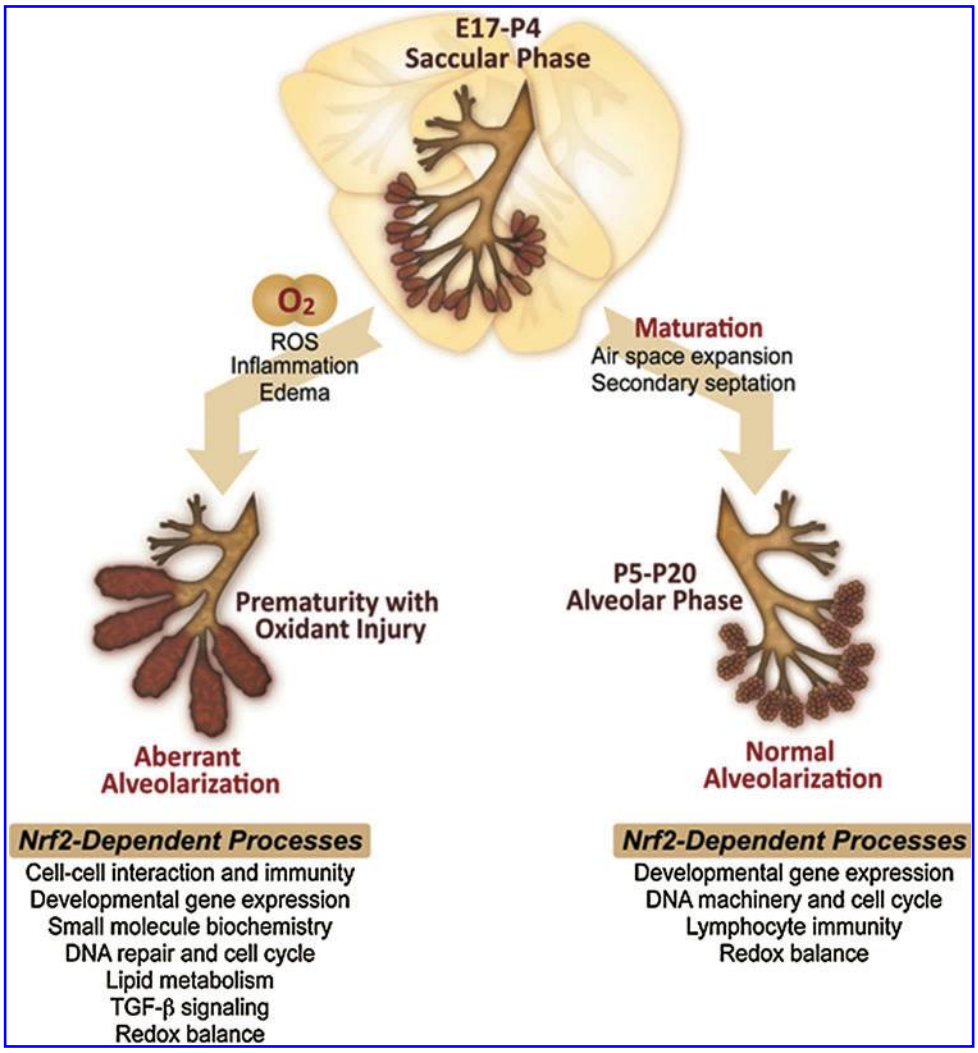

FIG. 7. Hypothetical schematics depicting proposed role for pulmonary Nrf2 in saccular-to-alveolar transition and hyperoxia-induced lung injury pathogenesis learned from mice. During early postnatal lung maturation and development, Nrf2 modulates expression of genes associated with DNA replication machinery, cell cycle regulation, development, and host defense and redox balance in mice. Abnormally high expression of genes for antigen presentation and T lymphocyte immunity are also evident in *Nrf2*$^{-/-}$ mice, indicating a role for Nrf2 in suppression of aberrant acquired immunity. Hyperoxia exposure during the late saccular phase causes oxidative injuries to lung proteins and lipids, and genomic and mitochondrial DNA damages are coupled to the tissue and protein edema, inflammation, cell death, and abnormal alveolar formation, which are similar to the bronchopulmonary dysplasia (BPD) phenotypes of prematurity. In *Nrf2*$^{-/-}$ lungs, these phenotypes are significantly augmented. Suppression of DNA repair device and redox capacity, interruption of cell cycle machinery and tissue development factors, alteration of lipid metabolism and small molecule biochemistry process, and potentiation of TGF-β signaling and fibrogenic factors in *Nrf2*$^{-/-}$ lungs in response to hyperoxia suggest functional roles for Nrf2 in the pathogenesis of BPD-like phenotypes. (To see this illustration in color the reader is referred to the web version of this article at www.liebertonline.com/ars)

and *Itga1*) were also Nrf2 dependent after hyperoxia exposure. Overall, observations imply a potential adverse effect of *Nrf2* deficiency on vessel development and endothelial differentiation in the saccular lung.

In conclusion, Nrf2 modulates genes involved in sustaining lung morphogenesis, cell growth machinery, and lymphocyte immunity during saccular lung maturation (Fig. 7). Nrf2 is also critical to protection of immature lungs from development of oxidative stress phenotypes caused by hyperoxia. Genetic loss of *Nrf2* caused augmented oxidation, inflammation, DNA lesions, and aberrant alveolarization of saccular lungs (Fig. 7). Transcriptome analysis suggested that Nrf2 in the immature lung protected against O_2 toxicity through regulation of DNA replication and cell cycle, various metabolism and small molecular process, and cell–cell interaction as well as redox homeostasis (Fig. 7). Functional bioinformatics elucidated downstream targets and *in vivo* validation of the role for *Gpx2* and *Marco* indicated that Nrf2 has a dual role in lung maturation and protection against hyperoxia-induced lung injury. Results contribute to our understanding of the role of Nrf2 in molecular processes of alveolarization and in lung diseases of prematurity, and may suggest a potential therapeutic role for specific Nrf2 inducers (agonists) in protection against human BPD.

Materials and Methods

Mice

Breeding colonies of *Nrf2*$^{-/-}$ (24), *Gpx2*$^{-/-}$ (19), and *Marco*$^{-/-}$ (2) mice were maintained in the National Institute of Environmental Health Sciences (NIEHS) animal facility. ICR (*Nrf2*$^{+/+}$) and C57BL/6J (*Gpx2*$^{+/+}$ and *Marco*$^{+/+}$) mice were purchased from Taconic and Jackson Laboratory, respectively. The mice and their neonate foster dams (Black Swiss or Swiss Webster; Taconic) were provided food (modified AIN-76A for *Nrf2*$^{+/+}$ and *Nrf2*$^{-/-}$, NIH-31 for others) and water *ad libitum*.

Inhalation exposure

Time-dated pregnant mice were cohabitated with appropriate time-pregnant foster dams on their delivery. Neonatal mice at P1 were placed in cages of a hyperoxia chamber, and exposed to 70% or 100% O_2 (National Welders) with their foster dams. Air control mice were placed in cages in room air for the same exposure duration. All animal use was approved by the NIEHS Animal Care and Use Committee. Additional detail is provided in the Supplementary Data.

Bronchoalveolar lavage

Whole lung of each neonate was lavaged *in situ* with Hank's balanced salt solution. The pooled BAL fluid returns were analyzed for total protein content and cell differentials as described in the Supplementary Data.

Histopathology and morphometry

Left lung tissues from each mouse were processed for hematoxylin and eosin staining, immunohistological detection of PCNA and TUNEL staining. Morphometric analysis was done to quantify the TUNEL-positive apoptotic cells (21) and the number of alveoli in the terminal respiratory unit (radial alveolar count, RAC) as a parameter of alveolar simplification (11, 18). Details are in the Supplementary Data.

Protein analysis

Lung proteins (20–100 μg) were subjected to Western blotting using specific primary antibodies (Supplementary Data). ARE binding activity of nuclear protein (5 μg) was determined by gel shift analysis on [γ^{32}P] ATP end-labeled consensus sequence (13).

Redox measurement

Total GSH levels were determined in lung homogenates (60 μg) by a colorimetric method (12). Oxidized protein amount was determined in lung protein aliquots (15 μg) by immunoblotting with anti-2,4-dinitrophenyl hydrazine (DNP) antibody after derivatization of carbonyl moieties using DNP (12). Amount of MDA was detected in BAL fluid (25 μl) for lipid peroxidation (OxiSelect TBARS Assay Kit; Cell Biolabs, Inc.). qPCR was performed to determine DNA base lesions in nuclear and mitochondrial genomes (40) as described in the Supplementary Data.

Microarray

Total lung RNA ($n=3$/group) was applied to Affymetrix mouse genome 430 V2.0 (Affymetrix, Inc.) in the NIEHS Microarray Core Facility. The array data were analyzed by GeneSpring (Agilent Technologies, Inc.), Ingenuity Pathway Analysis (IPA; Ingenuity Systems, Inc.), and Spotfire (TIBCO Software, Inc.) software. The microarray data are deposited in Gene Expression Omnibus (GEO, accession number: GSE29632) and in NIEHS Chemical Effects in Biological Systems (CEBS, accession number: 005-00003-0012-000-0). Greater details of microarray analysis are in the Supplementary Data.

Reverse transcription–polymerase chain reaction

qPCR (5) was performed on lung cDNA using 240 n*M* of gene-specific primers (Real Time Primers; LLC) in a 7700 Prism sequence detection system (Applied Biosystems). Semiquantitative PCR was done for Nrf2 messages (12).

Bioinformatics for ARE

Potential ARE sequences were determined in the 5 kb promoter regions using a PWM statistical model (48). Details are in the Supplementary Data.

Statistics

SigmaStat 3.0 software program (SPSS Science, Inc.) analyzed statistics. Individual *t*-test was done on TUNEL data ($p<0.05$). Two-way (Nrf2 mRNA expression) or three-way (other data) analysis of variance was followed by Student-Newman-Keuls test for *a posteriori* comparisons ($p<0.05$). Data were expressed as mean ± standard error of the mean (S.E.M).

Acknowledgments

This research was supported by the Intramural Research Program and Director's Challenge Program of the NIEHS, National Institutes of Health (NIH), Department of Health and Human Services. Hyperoxia exposures were conducted at the NIEHS. The authors thank Dr. Mary Grant and Mr. Norman Gage for installation of hyperoxia exposure chamber apparatus. The authors also thank Dr. Sue Edelstein of Image Associates for the professional artwork. We thank NIEHS Microarray Core personnel (Dr. Kevin Gerrish and Ms. Laura Wharey), and Ms. Laura Hall in the National Toxicology Program for submitting array data to GEO and NIEHS CEBS. Histopathologic evaluation of neonatal lung was performed by the pathologist Dr. Arlin Rogers (ILS, Inc., Research Triangle Park, NC) with support by Ms. Julie Foley of NIEHS Cellular and Molecular Pathology Branch. Drs. Pierre Buschel and Rick Paules of the NIEHS provided excellent critical review of the article.

Author Disclosure Statement

No competing financial interests exist.

References

1. Ahola T, Lapatto R, Raivio KO, Selander B, Stigson L, Jonsson B, Jonsbo F, Esberg G, Stovring S, Kjartansson S, Stiris T, Lossius K, Virkola K, and Fellman V. N-acetylcysteine does not prevent bronchopulmonary dysplasia in immature infants: a randomized controlled trial. *J Pediatr* 143: 713–719, 2003.
2. Arredouani M, Yang Z, Ning Y, Qin G, Soininen R, Tryggvason K, and Kobzik L. The scavenger receptor MARCO is required for lung defense against pneumococcal pneumonia and inhaled particles. *J Exp Med* 200: 267–272, 2004.

3. Baraldi E and Filippone M. Chronic lung disease after premature birth. *N Engl J Med* 357: 1946–1955, 2007.
4. Barker GF, Manzo ND, Cotich KL, Shone RK, and Waxman AB. DNA damage induced by hyperoxia: quantitation and correlation with lung injury. *Am J Respir Cell Mol Biol* 35: 277–288, 2006.
5. Bauer AK, Fostel J, Degraff LM, Rondini EA, Walker C, Grissom SF, Foley J, and Kleeberger SR. Transcriptomic analysis of pathways regulated by toll-like receptor 4 in a murine model of chronic pulmonary inflammation and carcinogenesis. *Mol Cancer* 8: 107, 2009.
6. Bowler RP, Barnes PJ, and Crapo JD. The role of oxidative stress in chronic obstructive pulmonary disease. *COPD* 1: 255–277, 2004.
7. Bry K, Whitsett JA, and Lappalainen U. IL-1beta disrupts postnatal lung morphogenesis in the mouse. *Am J Respir Cell Mol Biol* 36: 32–42, 2007.
8. Campbell MR, Chorley B, Wang X, Cho HY, Kleeberger SR, and Bell DA. Discovery of novel genomic targets in the NRF2-mediated antioxidant response pathway by ChIP-on-Chip and ChIP-seq. *Cancer Prev Res* 3 (1 Supplement): B51, 2010.
9. Chan K and Kan YW. Nrf2 is essential for protection against acute pulmonary injury in mice. *Proc Natl Acad Sci U S A* 96: 12731–12736, 1999.
10. Chessex P, Watson C, Kaczala GW, Rouleau T, Lavoie ME, Friel J, and Lavoie JC. Determinants of oxidant stress in extremely low birth weight premature infants. *Free Radic Biol Med* 49: 1380–1386, 2010.
11. Chetty A, Cao GJ, Severgnini M, Simon A, Warburton R, and Nielsen HC. Role of matrix metalloprotease-9 in hyperoxic injury in developing lung. *Am J Physiol Lung Cell Mol Physiol* 295: L584–L592, 2008.
12. Cho HY, Imani F, Miller-DeGraff L, Walters D, Melendi GA, Yamamoto M, Polack FP, and Kleeberger SR. Antiviral activity of Nrf2 in a murine model of respiratory syncytial virus disease. *Am J Respir Crit Care Med* 179: 138–150, 2009.
13. Cho HY, Jedlicka AE, Reddy SP, Kensler TW, Yamamoto M, Zhang LY, and Kleeberger SR. Role of NRF2 in protection against hyperoxic lung injury in mice. *Am J Respir Cell Mol Biol* 26: 175–182, 2002.
14. Cho HY, Jedlicka AE, Reddy SP, Zhang LY, Kensler TW, and Kleeberger SR. Linkage analysis of susceptibility to hyperoxia. Nrf2 is a candidate gene. *Am J Respir Cell Mol Biol* 26: 42–51, 2002.
15. Cho HY, Reddy SP, Debiase A, Yamamoto M, and Kleeberger SR. Gene expression profiling of NRF2-mediated protection against oxidative injury. *Free Radic Biol Med* 38: 325–343, 2005.
16. Cho HY, Reddy SP, Yamamoto M, and Kleeberger SR. The transcription factor NRF2 protects against pulmonary fibrosis. *FASEB J* 18: 1258–1260, 2004.
17. Chow CW, Herrera Abreu MT, Suzuki T, and Downey GP. Oxidative stress and acute lung injury. *Am J Respir Cell Mol Biol* 29: 427–431, 2003.
18. Emery JL and Mithal A. The number of alveoli in the terminal respiratory unit of man during late intrauterine life and childhood. *Arch Dis Child* 35: 544–547, 1960.
19. Esworthy RS, Mann JR, Sam M, and Chu FF. Low glutathione peroxidase activity in Gpx1 knockout mice protects jejunum crypts from gamma-irradiation damage. *Am J Physiol* 279: G426–G436, 2000.
20. Franco-Montoya ML, Bourbon JR, Durrmeyer X, Lorotte S, Jarreau PH, and Delacourt C. Pulmonary effects of keratinocyte growth factor in newborn rats exposed to hyperoxia. *Am J Physiol Lung Cell Mol Physiol* 297: L965–L976, 2009.
21. Gordon T and Harkema JR. Mucous cell metaplasia in the airways of rats exposed to machining fluids. *Fundam Appl Toxicol* 28: 274–282, 1995.
22. Halliwell B. Lipid peroxidation, antioxidants and cardiovascular disease: how should we move forward? *Cardiovasc Res* 47: 410–418, 2000.
23. Hirakawa H, Pierce RA, Bingol-Karakoc G, Karaaslan C, Weng M, Shi GP, Saad A, Weber E, Mariani TJ, Starcher B, Shapiro SD, and Cataltepe S. Cathepsin S deficiency confers protection from neonatal hyperoxia-induced lung injury. *Am J Respir Crit Care Med* 176: 778–785, 2007.
24. Itoh K, Chiba T, Takahashi S, Ishii T, Igarashi K, Katoh Y, Oyake T, Hayashi N, Satoh K, Hatayama I, Yamamoto M, and Nabeshima Y. An Nrf2/small Maf heterodimer mediates the induction of phase II detoxifying enzyme genes through antioxidant response elements. *Biochem Biophys Res Commun* 236: 313–322, 1997.
25. Jobe AH and Bancalari E. Bronchopulmonary dysplasia. *Am J Respir Crit Care Med* 163: 1723–1729, 2001.
26. Kensler TW, Curphey TJ, Maxiutenko Y, and Roebuck BD. Chemoprotection by organosulfur inducers of phase 2 enzymes: dithiolethiones and dithiins. *Drug Metabol Drug Interact* 17: 3–22, 2000.
27. Kunig AM, Balasubramaniam V, Markham NE, Morgan D, Montgomery G, Grover TR, and Abman SH. Recombinant human VEGF treatment enhances alveolarization after hyperoxic lung injury in neonatal rats. *Am J Physiol Lung Cell Mol Physiol* 289: L529–L535, 2005.
28. Li YJ, Takizawa H, Azuma A, Kohyama T, Yamauchi Y, Takahashi S, Yamamoto M, Kawada T, Kudoh S, and Sugawara I. Nrf2 is closely related to allergic airway inflammatory responses induced by low-dose diesel exhaust particles in mice. *Clin Immunol* 137: 234–241, 2010.
29. Lukkarinen H, Hogmalm A, Lappalainen U, and Bry K. Matrix metalloproteinase-9 deficiency worsens lung injury in a model of bronchopulmonary dysplasia. *Am J Respir Cell Mol Biol* 41: 59–68, 2009.
30. Malhotra D, Portales-Casamar E, Singh A, Srivastava S, Arenillas D, Happel C, Shyr C, Wakabayashi N, Kensler TW, Wasserman WW, and Biswal S. Global mapping of binding sites for Nrf2 identifies novel targets in cell survival response through ChIP-Seq profiling and network analysis. *Nucleic Acids Res* 38: 5718–5734, 2010.
31. McGrath-Morrow S, Lauer T, Yee M, Neptune E, Podowski M, Thimmulappa RK, O'Reilly M, and Biswal S. Nrf2 increases survival and attenuates alveolar growth inhibition in neonatal mice exposed to hyperoxia. *Am J Physiol Lung Cell Mol Physiol* 296: L565–L573, 2009.
32. Montuschi P, Curro D, Ragazzoni E, Preziosi P, and Ciabattoni G. Anaphylaxis increases 8-iso-prostaglandin F2alpha release from guinea-pig lung *in vitro*. *Eur J Pharmcol* 365: 59–64, 1999.
33. Northway WH Jr., Moss RB, Carlisle KB, Parker BR, Popp RL, Pitlick PT, Eichler I, Lamm RL, and Brown BW Jr. Late pulmonary sequelae of bronchopulmonary dysplasia. *N Engl J Med* 323: 1793–1799, 1990.
34. Nozik-Grayck E, Dieterle CS, Piantadosi CA, Enghild JJ, and Oury TD. Secretion of extracellular superoxide dismutase in neonatal lungs. *Am J Physiol Lung Cell Mol Physiol* 279: L977–L984, 2000.
35. Panayiotidis MI, Rancourt RC, Pappa A, and White CW. Effect of cell cycle growth arrest on global DNA methylation

status in human lung epithelial-like (A549) cells. *In Vivo* 20: 861–865, 2006.
36. Rangasamy T, Cho CY, Thimmulappa RK, Zhen L, Srisuma SS, Kensler TW, Yamamoto M, Petrache I, Tuder RM, and Biswal S. Genetic ablation of Nrf2 enhances susceptibility to cigarette smoke-induced emphysema in mice. *J Clin Invest* 114: 1248–1259, 2004.
37. Rangasamy T, Guo J, Mitzner WA, Roman J, Singh A, Fryer AD, Yamamoto M, Kensler TW, Tuder RM, Georas SN, and Biswal S. Disruption of Nrf2 enhances susceptibility to severe airway inflammation and asthma in mice. *J Exp Med* 202: 47–59, 2005.
38. Reddy NM, Kleeberger SR, Kensler TW, Yamamoto M, Hassoun PM, and Reddy SP. Disruption of Nrf2 impairs the resolution of hyperoxia-induced acute lung injury and inflammation in mice. *J Immunol* 182: 7264–7271, 2009.
39. Rickett GM and Kelly FJ. Developmental expression of antioxidant enzymes in guinea pig lung and liver. *Development* 108: 331–336, 1990.
40. Santos JH, Meyer JN, Mandavilli BS, and Van Houten B. Quantitative PCR-based measurement of nuclear and mitochondrial DNA damage and repair in mammalian cells. *Methods Mol Biol* 314: 183–199, 2006.
41. Sasaki H, Sato H, Kuriyama-Matsumura K, Sato K, Maebara K, Wang H, Tamba M, Itoh K, Yamamoto M, and Bannai S. Electrophile response element-mediated induction of the cystine/glutamate exchange transporter gene expression. *J Biol Chem* 277: 44765–44771, 2002.
42. Stenmark KR and Abman SH. Lung vascular development: implications for the pathogenesis of bronchopulmonary dysplasia. *Annu Rev Physiol* 67: 623–661, 2005.
43. Thebaud B, Ladha F, Michelakis ED, Sawicka M, Thurston G, Eaton F, Hashimoto K, Harry G, Haromy A, Korbutt G, and Archer SL. Vascular endothelial growth factor gene therapy increases survival, promotes lung angiogenesis, and prevents alveolar damage in hyperoxia-induced lung injury: evidence that angiogenesis participates in alveolarization. *Circulation* 112: 2477–2486, 2005.
44. Thimmulappa RK, Lee H, Rangasamy T, Reddy SP, Yamamoto M, Kensler TW, and Biswal S. Nrf2 is a critical regulator of the innate immune response and survival during experimental sepsis. *J Clin Invest* 116: 984–995, 2006.
45. Tin W and Wiswell TE. Drug therapies in bronchopulmonary dysplasia: debunking the myths. *Semin Fetal Neonatal Med* 14: 383–390, 2009.
46. Vicencio AG, Lee CG, Cho SJ, Eickelberg O, Chuu Y, Haddad GG, and Elias JA. Conditional overexpression of bioactive transforming growth factor-beta1 in neonatal mouse lung: a new model for bronchopulmonary dysplasia? *Am J Respir Cell Mol Biol* 31: 650–656, 2004.
47. Walsh MC, Szefler S, Davis J, Allen M, Van Marter L, Abman S, Blackmon L, and Jobe A. Summary proceedings from the bronchopulmonary dysplasia group. *Pediatrics* 117: S52–S56, 2006.
48. Wang X, Tomso DJ, Chorley BN, Cho HY, Cheung VG, Kleeberger SR, and Bell DA. Identification of polymorphic antioxidant response elements in the human genome. *Hum Mol Genet* 16: 1188–1200, 2007.
49. Warner BB, Stuart LA, Papes RA, and Wispe JR. Functional and pathological effects of prolonged hyperoxia in neonatal mice. *Am J Physiol* 275: L110–L117, 1998.
50. Yue X, Fu J, Xue X, Gao H, Liu D, Zong Z, Wang W, Li H, and Yuan Z. Detection of p16 promoter methylation in premature rats with chronic lung disease induced by hyperoxia. *Pediatr Int* 52: 520–526, 2010.

Address correspondence to:
Dr. Hye-Youn Cho
Laboratory of Respiratory Biology
National Institute of Environmental Health Sciences
National Institutes of Health
111 TW Alexander Dr., Building 101, MD D-201
Research Triangle Park, NC 27709

E-mail: cho2@niehs.nih.gov

Date of first submission to ARS Central, September 20, 2011; date of final revised submission, March 6, 2012; date of acceptance, March 6, 2012.

Abbreviations Used

Akr1b8 = aldo-keto reductase family 1, member B8 (murine, gene)
ANG = angiogenin
ANGPT2 = angiopoietin-2
ANOVA = analysis of variance
Aox1 = aldehyde oxidase 1 (murine, gene)
ARE = antioxidant response element
BAL = bronchoalveolar lavage
BPD = bronchopulmonary dysplasia
CEBS = Chemical Effects in Biological Systems
Clstn2 = calsyntenin 2 (murine, gene)
Creg1 = cellular repressor of E1A-stimulated genes 1 (murine, gene)
DNP = 2,4-dinitrophenyl hydrazine
Egr2 = early growth response 2 (murine, gene)
Gclc = glutamate cysteine ligase, catalytic subunit (murine, gene)
GCS = glutamate cysteine ligase
GEO = gene expression omnibus
GI = gene identification
GPx2 = glutathione peroxidase 2
GSH = glutathione
GST = glutathione S-transferase
H&E = hematoxylin and eosin
H2-D1 = histocompatibility 2, D region locus 1 (murine, gene)
H2-Q1 = histocompatibility 2, Q region locus 1 (murine, gene)
HBSS = Hank's balanced salt solution
Hc = hemolytic complement (murine, gene)
Ho1 = heme oxygenase-1 (murine, gene)
Inta4 = integrin alpha 4 (murine, gene)
IPA = ingenuity pathway analysis
Jag1 = jagged 1 (murine, gene)
KO = knockout
LDH = lactate dehydrogenase
MARCO = macrophage receptor with collagenous structure
MDA = malondialdehyde
MHCII = major histocompatibility complex, class II
MMPs = matrix metalloproteases
MS score = matrix similarity score
Mtr = 5-methyltetrahydrofolate-homocysteine methyltransferase (murine, gene)

Abbreviations Used (Cont.)

NF-κB = nuclear factor κB
NIEHS = National Institute of Environmental Health Sciences
NIH = National Institutes of Health
NQO1, *Nqo1* = NAD(P)H:quinone oxidoreductase 1
Nrf2, Nfe2l2 = NF-E2 related factor 2
PCNA = proliferating cell nuclear antigen
PDGF = platelet-derived growth factor
qRT-PCR = quantitative reverse transcription–polymerase chain reaction
RAC = radial alveolar count
Rad51 = RAD51 homolog (murine, gene)
ROS = reactive oxygen species
SEM = standard error of the mean
Slc7a11 = solute carrier family 7 (cationic amino acid transporter, y+ system), member 11
SOD = superoxide dismutase
TGF-β = transforming growth factor beta
TSS = transcription start site
TUNEL = terminal deoxynucleotidyl transferase-mediated dUTP nick-end labeling
TXNRD = thioredoxin reductase
VEGF = vascular endothelial growth factor
WT = wild-type